Multiple neuronal networks coordinate *Hydra* mechanosensory behavior

Krishna N. Badhiwala[1], Abby S. Primack[2], Celina E. Juliano[2], Jacob T. Robinson*[1,3,4]

1. Department of Bioengineering, Rice University, 6100 Main Street, Houston, Texas 77005
2. Department of Molecular and Cellular Biology, University of California, Davis, CA, USA.
3. Department of Electrical and Computer Engineering, Rice University, 6100 Main Street, Houston, Texas 77005
4. Department of Neuroscience, Baylor College of Medicine, One Baylor Plaza, Houston, Texas, 77030

*Correspondence to: jtrobinson@rice.edu.

Abstract

Hydra vulgaris is an emerging model organism for neuroscience due to its small size, transparency, genetic tractability, and regenerative nervous system; however, fundamental properties of its sensorimotor behaviors remain unknown. Here, we use microfluidic devices combined with fluorescent calcium imaging and surgical resectioning to study how the diffuse nervous system coordinates *Hydra*'s mechanosensory response. Mechanical stimuli cause animals to contract, and we find this response relies on at least two distinct networks of neurons in the oral and aboral regions of the animal. Different activity patterns arise in these networks depending on whether the animal is contracting spontaneously or contracting in response to mechanical stimulation. Together, these findings improve our understanding of how *Hydra*'s

diffuse nervous system coordinates sensorimotor behaviors. These insights help reveal how sensory information is processed in an animal with a diffuse, radially symmetric neural architecture unlike the dense, bilaterally symmetric nervous systems found in most model organisms.

Introduction

Discovering the fundamental principles of neural activity and behaviors requires studying the nervous systems of diverse organisms. Animals have evolved different neural structures like the nerve net (e.g. *Hydra*), nerve cords and ganglia (e.g. *C. elegans*, *Aplysia*, planaria), and brain (e.g. *Drosophila*, zebrafish, rodents, and primates). Despite the vastly different structures, many behaviors are conserved across species, including sensorimotor responses[1–6] and sleep[7–15]. By comparing neural circuits that support similar behaviors despite different architectures, we can discover organizational principles of neural circuits that reflect millions of years of evolutionary pressure. While there are many potential organisms that would support this type of comparative neuroscience, only a small group of animals have the qualities to support laboratory experiments: short generation span, ease of breeding and manipulation in laboratory conditions, small and compact size, optical transparency, and a well-developed genetic toolkit with a complete spatial and molecular map of the nervous system.

Transparent, millimeter-sized animals in particular offer a number of advantages for neuroscientists because it is possible to image neural activity throughout the entire nervous system using genetically-encoded calcium or voltage-sensitive fluorescent proteins[16–25]. In addition, some millimeter-sized animals are compatible with microfluidic devices for precise

51 environmental control and microscopy techniques that offer cellular-resolution functional
52 imaging of the entire nervous system. These properties, combined with genetic tractability,
53 provide a powerful way of revealing neuronal dynamics across the entire nervous system (not
54 just a small region) during behaviors. For instance, whole nervous system imaging of confined
55 or freely moving animals has revealed the neuronal dynamics underlying locomotion[19,26] and
56 sensory motivated global state transitions in *C. elegans*[27,28], responses to noxious odor and
57 visuomotor behaviors in zebrafish[19–24], responses to light and odor in *Drosophila*[18,29], and
58 neuronal ensembles correlated with basal behaviors and response to light in *Hydra*[30,31].
59
60 *Hydra* is unique among the small, transparent organisms discussed above due to its
61 regenerative ability and highly dynamic nervous system. While most small, transparent model
62 systems (like *C. elegans* or zebrafish larvae) suffer permanent behavioral deficits from the loss
63 of one or a few neurons[32–36], *Hydra* can completely recover from a significant neuronal loss to
64 regain normal contractile behavior in as little as ~ 48 hours[37–39]. This radially symmetric
65 freshwater cnidarian has a nervous system composed of two diffuse networks of neurons, one
66 embedded in the endoderm and another embedded in the ectoderm[40,41]. While *Hydra's* diffuse
67 nerve net is highly dynamic with continuous cellular turnover and migration[42,43], regions with
68 increased neuron density resembling nerve rings have a comparatively lower neuronal turnover
69 (Figure 1a)[44–47]. One of these regions is in the oral end in the apex above the ring of tentacles
70 ("hypostomal nerve ring"), and another is in the aboral end in the foot ("peduncle nerve ring")
71 (Figure 1a). Recent single-cell RNA sequencing has provided a complete molecular and spatial
72 map of the *Hydra* nervous system, including identification of unique cell-type specific biomarkers
73 to generate new transgenic models[48]. This existing molecular and spatial map of the nervous
74 system suggests there is no overlap in the neuronal cell types that make up the hypostomal and
75 peduncle nerve rings, and the distribution of the cell types varies along the length of the body
76 (Figure 1b). Finally, the demonstration of microfluidic and transgenic tools combined with

Hydra's dynamic yet 'simple' neural architecture has enabled observations of basal and sensory motivated behaviors in the regenerating nervous system[31].

To better establish *Hydra* as a model organism for comparative neuroscience, it is critical to understand their basic sensorimotor behaviors, such as response to touch. While it is well documented that *Hydra* contract when mechanically agitated or poked with a pipette[49–53], we found no quantitative reports of how this behavior depends on stimulus intensity or is mediated by neural activity. Although significant insights in *Hydra* behavior have been made over the last several decades with simple methodologies and manual observations, including that the tentacles and/or the hypostome are needed for mechanosensory response, these experiments lack quantitative characterization of neuronal or behavioral response. Forceps-induced touch allows local stimulation, but it is difficult to control the force applied manually[54,55]. While stimulation with mechanical agitation allows control over stimulus intensity, these observations are limited to changes in body lengths[52].

Here, we use whole animal functional imaging combined with resection studies to discover that despite the apparently diffuse nerve net in *Hydra*, these animals process sensorimotor responses in specialized regional networks. To study the mechanosensory response, we first developed a microfluidic system to apply a local mechanical stimulus and quantify *Hydra's* behavioral and neural response. We then measured these responses in the absence of select regions of the body and found at least one of the neuron-rich regions, the hypostome (oral) or the peduncle (aboral), is required to coordinate spontaneous contractions, though the oral network plays a more significant role. We found a significant reduction in the mechanosensory response with the removal of the hypostome, the region where sensory information is likely processed. These sensorimotor experiments combined with whole-animal neural and

102 epitheliomuscular imaging reveal that *Hydra* is capable of receiving sensory information along
103 the body column; however, the oral region is necessary for coordinating the motor response.
104
105

106 Results

107

108 *Hydra's* mechanosensory response is dependent on stimulus intensity

109

110 To better understand sensory information processing in *Hydra*, we developed a double-layer
111 microfluidic system that can apply a local mechanical stimulus while we image the response of
112 the entire nervous system using fluorescence microscopy (Figure 2, Video 1). This local
113 mechanical stimulation is made possible by push-down microfluidic valves (Figure 2a) that
114 deliver mechanical stimuli to a portion of the *Hydra* body with precise temporal and spatial
115 control (see "Methods"). For all experiments, we pressurized a valve (400 μm diameter) that
116 was directly above the animal (for 1 sec every 31 sec, see "Methods") to stimulate the body
117 column while simultaneously performing functional calcium imaging (Figure 2b). We selected
118 the middle of the body for stimulation region to help ensure that we stimulated roughly the same
119 region of the animal throughout each experiment. This choice was based on the observation
120 that the body column region was relatively stationary, whereas the oral and aboral extremities
121 had large displacements during body contractions and elongations.
122
123 Experiments showed that this stimulation paradigm delivered a local mechanical stimulation with
124 most of the mechanical force localized to a radius of approximately 250 μm around the
125 microfluidic valve. To measure the locality of this stimulus we performed an experiment using
126 transgenic *Hydra* (nGreen)[48] expressing GFP pan-neuronally (and in neural progenitors) and

127 tracked the position and fluorescence intensity (GFP) from individual neurons during mechanical
128 stimulation (N = 222 neurons over 1 min). When the microfluidic valve was pressurized to
129 deliver mechanical stimulation, we found significantly increased average cellular (or tissue)
130 displacement ($p < 0.001$). Further analysis of the cellular movements showed the spatial
131 distribution of mechanical force from the stimulation was primarily experienced by the neurons
132 directly under the valve (Figure 2 – Figure Supplement 1). Specifically, we found that the tissue
133 directly below the valve was compressed (z direction) when mechanically stimulated - the
134 neurons directly under the valve had a small magnitude of lateral (x-y direction) displacement.
135 The tissue bordering the valve was stretched away from the valve center - the neurons in the
136 neighboring regions around the valve had the largest lateral displacement. This lateral
137 displacement decreased for neurons that were farther from the center of the valve. Neurons
138 more than 750 μm from the microfluidic valve center showed a negligible displacement of less
139 than 5 μm (95% CI lower bound = 5.8 μm), which is ~550% less than the displacement of
140 neurons bordering the valve.
141
142 Having established our method to provide local mechanical stimuli, we characterized *Hydra's*
143 sensitivity to local touch and the associated neural response. We performed experiments using
144 transgenic *Hydra* expressing GCaMP6s in neurons[30]. When we delivered mechanical stimuli,
145 we found bright calcium signals generated by a small number of neurons in the hypostome and
146 body column and a striking co-activation of many neurons in the ectodermal peduncle nerve ring
147 (Figure 2b, Video 2, 3). This nerve ring activity appeared as either a single bright calcium spike
148 (or "contraction pulse") or a volley of bright calcium spikes (or "contraction burst"). We also
149 found that the calcium-sensitive fluorescence averaged over a region of interest (ROI)
150 surrounding the peduncle faithfully represented the contraction pulses and bursts measured
151 from individual neurons (Figure 2 - Figure Supplement 2). When we analyzed single neuron
152 calcium dynamics from this peduncle nerve ring, we found extremely high correlated activity as

153 previously reported for contractions pulses and bursts (Figure 2 - Figure Supplement 2)[30,31].
154 Given the similarity of these data between large and small ROIs, we chose to use the peduncle
155 ROI to measure neuronal contraction bursts and pulses because it does not require single-
156 neuron tracking, which significantly increased the throughput of our data analysis. We further
157 confirmed that this signal is not the result of motion artifacts by measuring fluorescence from
158 *Hydra* (nGreen) that express GFP pan-neuronally using a similar ROI. In that case we did not
159 see the strong fluorescence signals associated with contraction pulses and bursts (Figure 2 –
160 Figure Supplement 3e-f). Body length proved to be an unreliable quantification of contractions
161 due to the stimulation artifacts (Figure 2 - Figure Supplement 3d); however, we were able to
162 accurately measure muscle activity associated with contractions by imaging calcium spikes in
163 the epithelial muscle cells (Figure 2 - Figure Supplement 4, 5 and Video 4, 5). Based on these
164 experiments, we define *Hydra's* "mechanosensory response" as calcium spikes in neural activity
165 from the peduncle ROI and the associated calcium spikes in the epithelial muscles from the
166 whole body if they occur within one second of mechanical stimulation onset (Figure 2c, d and
167 Figure 2 – Figure Supplement 6).
168
169 Using the neuronal fluorescence calcium imaging described above, we found that the probability
170 of the mechanosensory response depends on the intensity of the stimulus, which is consistent
171 with many psychometric functions (Figure 2e). *Hydra* were five times more likely to contract
172 within one second of receiving a strong mechanical stimulus than during a random one second
173 interval without a stimulus (stimulus valve pressure 20 and 25 psi; response probability = 0.60 ±
174 0.06 and 0.77 ± 0.08, mean ± SEM, respectively; no stimulus valve pressure = 0 psi; response
175 probability = 0.11 ± 0.01, mean ± SEM; Figure 2e, h). During mild stimuli, there was a slight
176 increase (~ 2x) in response probability above the spontaneous activity, although this increase
177 was not statistically significant compared to spontaneous contraction bursts or pulses (valve
178 pressure 10 and 15 psi; response probability = 0.23 ± 0.01 and 0.24 ± 0.03, mean ± SEM,

179 respectively; Figure 2e, h). We found that *Hydra* did not respond to a weak mechanical stimulus
180 that corresponded to a valve pressure of 5 psi (response probability = 0.09 ± 0.02, mean ±
181 SEM; Figure 2e, h).
182
183 Further analysis of the calcium activity pattern revealed that the single contraction pulses
184 (calcium spikes in the peduncle neurons) were more frequent when we repeated mechanical
185 stimulation every 31 seconds for one hour. While spontaneous contraction pulses or bursts
186 were observed roughly once every minute in microfluidics, when we stimulated *Hydra* with a
187 strong mechanical stimuli, we found that the frequency nearly matched the 31 sec between
188 stimuli (Interval between spontaneous contraction bursts or pulses = 72.98 sec ± 4.58, mean ±
189 SEM; 66.68 ± 5.73 sec median ± SE; Interval between stimulated contraction bursts or pulses =
190 20 psi, 38.28 ± 1.77 sec, mean ± SEM; 31.14 ± 2.21 sec, median ± SE; 25 psi, 32.20 ± 1.04
191 sec, mean ± SEM; 31.14 ± 1.30 sec, median ± SE; Figure 2f,h). While the majority of
192 spontaneous calcium spikes formed bursts, stimulated calcium spikes were roughly three times
193 more likely to be a single contraction pulses (Percentage of spontaneous spiking activity that is
194 a single contraction pulse = 0psi, 16.87 ± 5.38 % mean ± SEM; Percentage of stimulated
195 spiking activity that is a single contraction pulse = 20 psi, 56.84 ± 2.48%; 25psi, 62.50 ± 5.23 %,
196 mean ± SEM; Figure 2g, h).
197
198
199 ***Hydra* sensitivity to mechanical stimuli is lowest near the aboral end**
200
201 Because of the diffuse neural architecture of *Hydra*, we expected each patch of *Hydra* tissue to
202 be equally responsive to mechanical stimuli. However, when we stimulated transgenic *Hydra*
203 expressing GCaMP6s (N = 3 whole animals, stimulated 40 times per region with 22 psi) at three
204 different regions along their body (oral, middle body and aboral, stimulated 40 times at each

205 region with 22psi), we found the aboral end of *Hydra* to be less sensitive than the center of the
206 body (aboral region response probability = 0.1 ± 0.025; mid-body region response probability =
207 0.42 ± 0.025; mean ± SEM; $p < 0.01$; Figure 2 - Supplement figure 7a). Epitheliomuscular
208 calcium imaging (N = 8 whole animals expressing GCaMP7b in ectodermal epitheliomuscular
209 cells, stimulated 40 times in body column region with 22psi) also showed that the sensitivity to
210 mechanical stimulation generally decreases towards the aboral end of the *Hydra* (Figure 2 –
211 Supplement figure 7b). Furthermore, we found that the difference in sensitivity along the body
212 was not an artifact due to differently sized *Hydra* experiencing different pressures from the
213 microfluidic valves. We observed no statistically significant trend between animal size and
214 response probability (Figure 2 – Supplement figure 7c). These findings, combined with the
215 transcriptional analysis and in-situ hybridizations that indicate higher density of sensory neurons
216 in the oral half of the *Hydra*[48], suggest the oral end may be more sensitive to mechanical stimuli.
217 Unlike other organisms that have unique motor responses like reversals or acceleration
218 depending on the location of mechanical stimuli (e.g. *C. elegans*)[56,57], we observed that the
219 same motor program was initiated regardless of where on the body the animal was touched.
220 The only difference we observed was the fact that the response probability depended on where
221 along the oral and aboral axis we delivered the mechanical stimulus.
222
223
224 ***Hydra*'s mechanosensory response is mediated by electrically-coupled cells**
225
226 Based on the latency of the mechanosensory response, we hypothesized that sensorimotor
227 information is transmitted by electrical activity in the *Hydra* and not by passive calcium diffusion
228 through ectodermal cells. This hypothesis is supported by the fact that aneural *Hydra,* which no
229 longer spontaneously contract in absence of stimuli, are capable of aversive contractile
230 response to touch, however, their responses are slow and require strong mechanical

231 stimulus[54,55]. To further test our hypothesis, we created a transgenic *Hydra* strain that expresses
232 the calcium indicator GCaMP7b (under the EF1α promoter, see "Methods") in the ectodermal
233 epitheliomuscular cells. With this transgenic line we measured contraction pulses and
234 contraction bursts by averaging calcium activity in all epitheliomuscular cells (Figure 2 – Figure
235 Supplement 3, 5). We hypothesized that if the mechanosensory response was primarily
236 mediated by calcium diffusion through epitheliomuscular cells, we would expect to see
237 propagation of calcium activity from the site of the stimulation. However, this was not the case;
238 we observed fast propagation of calcium activity throughout the entire ectoderm. Imaging
239 calcium activity in the peduncle neurons showed that changes in neural activity correlated with
240 the observed changes in epithelial muscle cells with increasing stimulus intensity (Figure 2 and
241 Figure 2 – Figure Supplement 5). This suggests that the mechanosensory response is indeed
242 mediated by the electrically-coupled cells. Although *Hydra*'s behavioral responses are slow
243 compared to other invertebrates, the 0.5 sec average response time in our data could not be
244 explained by calcium diffusion alone, which would take ~100 sec to travel the average distance
245 of ~0.5-1 mm between the stimulation site and the peduncle or hypostome (Figure 2 – Figure
246 Supplement 8a). Our data show the calcium signals from the peduncle neurons or ectodermal
247 muscles start increasing within ~0.1-0.2 sec following stimulation onset, reaching peak
248 fluorescence at ~0.5-0.6 sec regardless of the stimulus intensity (Figure 2 – Figure Supplement
249 8b-e). We found no difference in the calcium response times between neural and muscle
250 calcium imaging, though this could be influenced by the dynamics of the calcium indicator,
251 which typically cannot give information about latencies less than 50 ms[17].
252
253 **Aboral neurons are not necessary for mechanosensory response in *Hydra***
254
255 Having quantitatively established *Hydra's* sensorimotor response to mechanical stimuli, we next
256 asked if specific regions of the nervous system play primary roles in mediating this response.

257 Patch-clamp electrophysiology of individual neurons in *Hydra* has thus far been unsuccessful
258 despite attempts by many research groups, and minimally invasive, cell-type specific
259 neuromodulation techniques such as optogenetics have yet to be developed for *Hydra*.
260 However, the animal's regenerative abilities allow us to resect large portions of tissue without
261 killing the animal, thus we can borrow from the tradition of lesioning brain regions to study their
262 functions[52,58–61].
263
264 Because the *Hydra* body plan is radially symmetric with cell types primarily varying along the
265 oral-aboral axis of the body column (Figure 1), we chose to make axial cuts across the body
266 column to remove select neuronal populations from the animal. Our rationale was that these
267 resections would remove entire or nearly entire groups of neuronal cell types. We then allowed
268 ~6-12 hours for the animal to recover. This recovery time helps to reduce the confounding
269 contributions from initial tissue regeneration and allows animals to recover enough to tolerate
270 microfluidic immobilization. This period is long enough to allow the wounds to close, the
271 molecular response to injury to be completed[62,63], and the initial molecular events of
272 regeneration to start; but it is *not* long enough for the animal to regenerate lost neurons, which
273 takes approximately 30-72 hours (Figure 3 – Figure Supplement 1)[37,61,64,65]. We confirmed that
274 6-12 hours after resection the animals indeed showed loss of specific neuronal cell types by
275 measuring the expression levels of subtype-specific neuronal markers via qPCR (Figure 3 -
276 Figure Supplement 2). To limit the stress from microfluidic immobilization that could exacerbate
277 the resection wounds and affect activity, we shortened the duration of these experiments for the
278 majority of the animals (40 min total, 20 min of no stimulation, 20 min of stimulation - valve on 1
279 sec at 22 psi or 0 psi, off 30 sec). Only three animals per each condition (stimulated and non-
280 stimulated, and 5 different resections) were experimented on with a longer duration protocol as
281 used previously (100 min total, 20 min no stimulation, 60 min of stimulation - valve on 1 sec at
282 22 psi or 0 psi, off 30 sec, 20 min no stimulation; Figure 3 - Figure Supplement 3).

283

284 We began resection studies by removing the peduncle and basal disk to create a “footless”
285 *Hydra.* We hypothesized that aboral neurons may be important for coordinating and enhancing
286 body contractions (Figure 3). We based this hypothesis on the fact that aboral neuron activity
287 has a strong correlation with body contractions[30,31]. In addition, the neuropeptide Hym-176C has
288 been shown to induce ectodermal muscle contractions and is selectively expressed in the
289 ectodermal peduncle neurons[48,66–68]. Finally, the presence of gap junction protein innexin-2 in
290 aboral neurons could facilitate fast electrical conductions that allows these neurons to fire
291 synchronously[48,55]. This could be necessary for enhancing neuromuscular signaling for body
292 contractions. Because “footless” *Hydra* lacked peduncle neurons that we had used previously to
293 measure contraction pulses and bursts (Figure 3 - Supplement Figure 3d-f, and Video 6-9), we
294 performed these experiments using a transgenic *Hydra* line expressing GCaMP7b in the
295 ectodermal epitheliomuscular cells, which allowed us to measure contraction pulses and bursts
296 by averaging calcium activity in all the epitheliomuscular cells (using whole frame ROI which is
297 more robust to motion artifacts than peduncle ROI; Figure 2 - Figure Supplement 3, Figure 3a,b,
298 Figure 3 – Figure Supplement 3).

299

300 Because neurons in the foot fire synchronously with body contractions, we expected “footless”
301 animals to show significant changes in contraction behaviors (calcium spiking activity) to be
302 significantly affected by their removal[30,31,69], but this was not what we observed. Surprisingly, our
303 experiments with “footless” animals showed that the aboral nerve ring was not required to
304 regulate spontaneous contraction bursts or pulses or mechanosensory responses. After we
305 removed the peduncle network in *Hydra*, we found the increase in contraction burst or pulse
306 activity with stimuli (or mechanosensory response) in “footless” individuals was similar to the
307 increase in activity observed in whole individuals (“Footless” N = 8 animals stimulated 20 min,
308 Cohen’s d = 1.89, Cliff’s delta = 0.81, $p < 0.01$); Whole N = 8 animals stimulated 20 min,

Cohen's d = 1.80, Cliff's delta = 1.00, $p < 0.01$; Fig 3b,c). Furthermore, we found no significant difference in either the spontaneous contraction probability or the mechanosensory response probability of "footless" animals and whole animals ("Footless" N = 3 animals not stimulated, spontaneous contraction probability = 0.13 ± 0.01, mean ± SEM; "Footless" N = 3 animals stimulated for 60 min, mechanosensory response probability = 0.88 ± 0.05, mean ± SEM) (Whole N = 3 animals not stimulated, spontaneous contraction probability = 0.15 ± 0.01, mean ± SEM; Whole N = 3 animals stimulated for 60 min, mechanosensory response probability = 0.73 ± 0.07, mean ± SEM; Figure 3 - Figure Supplement 3b,c, Video 4, 5,10, and 11).

Oral neurons play a major role in mechanosensory response in *Hydra*

While the mechanosensory response in *Hydra* remained unaffected with the removal of the aboral nerve ring, we found that removal of the hypostome and tentacles (or "headless" *Hydra*) resulted in significant changes in both the mechanosensory response and spontaneous contraction bursts or pulses. When we measured the mechanosensory response in "headless" *Hydra,* we found that the animals still responded to mechanical stimulation with a significant increase in their contraction bursts or pulses, however, they did so with a lower magnitude compared to whole and "footless" individuals ("Headless" N = 8 animals stimulated for 20 min, $p < 0.01$, Cohen's d = 1.37, Cliff's delta = 1.00; Figure 3b, c). Specifically, the "headless" *Hydra* responded with (> 2x) lower probability compared to whole animals, and they also showed a (> 3x) lower probability of spontaneous contraction bursts and pulses ("Headless" N = 3 animals stimulated for 60 min, mechanosensory response probability = 0.29 ± 0.02, mean ± SEM; "Headless" N = 3 animals not stimulated, spontaneous contraction probability = 0.05 ± 0.01, mean ± SEM; Figure 3 - Figure Supplement 3b, c, Video 12 and 13).

To verify the reduction in mechanical response probability was specific to removing the oral network of neurons, and not simply the result of injury, we performed experiments with animals that we cut longitudinally along the body axis (“bisected” *Hydra*) to remove approximately the same amount of tissue while preserving the neuronal subtypes in both the oral and aboral networks. We found that these longitudinally “bisected” animals showed mechanosensory responses that were not significantly different from that of the whole, “headless”, or “footless” animals (“Bisected” N = 3 animals stimulated for 60 min, mechanosensory response probability = 0.54 ± 0.14, mean ± SEM; Figure 3 - Figure Supplement 3b, c). However, the magnitude of increase in contraction bursts or pulses activity due to stimulation in “bisected” individuals, though lower than whole and “footless” individuals, was larger than “headless” individuals (“Bisected” N = 8 animals stimulated for 20 min, $p < 0.001$, Cohen’s d = 2.32, Cliff’s delta = 1.0). This suggests that our observations in “headless” *Hydra* indeed depended upon the types of neurons removed during the headless resection and not simply an injury response. We also found that these longitudinally “bisected” animals had a lower probability of spontaneous contraction bursts or pulses than the whole animals but higher than “headless” animals. This suggests that the entire network needs to be intact for normal contraction bursts or pulses activity, and the loss of roughly half the network leads to some reduction in contractile activity (“Bisected” N = 3 animals not stimulated, spontaneous contraction probability = 0.08 ± 0.02, mean ± SEM; Figure 3 - Figure Supplement 3b, c Video 14 and 15).

We next asked if the body column alone is sufficient to mediate the mechanosensory response. To answer this question, we completely removed both oral and aboral regions. In “body column” animals, we found significant reduction in both the mechanosensory response and spontaneous contraction bursts and pulses relative to whole animals. The “body column” animals had a mechanosensory response probability that was not different from the mechanosensory response in “headless” animals, while the spontaneous contraction bursts and pulses probability

361 was lower compared to that of “headless” animals (“Body column” N = 3 animals stimulated for
362 60 min, mechanosensory response probability = 0.19 ± 0.08; “Body column” N = 3 animals not
363 stimulated, spontaneous contraction probability = 0.02 ± 0.01 mean ± SEM; Figure 3 - Figure
364 Supplement 3b,c). Although we found a significant increase in contraction bursts and pulses
365 with stimulation as compared to spontaneous contraction bursts and pulses activity in “body
366 column” individuals similar to all resections, the magnitude of the increase was the lowest in
367 “body column” animals (even lower than “headless” animals) (“Body column” N = 6 animals
368 stimulated for 20 min, $p < 0.05$, Cohen’s d = 1.10, Cliff’s delta = 0.50; Figure 3b, c, Video 16 and
369 17). Moreover, we did not observe significant increases in contraction bursts and pulses over
370 the same time period (comparing activity from 0 - 20 min with activity from 20 - 40 min, see
371 “Methods”) in non-stimulated animals, suggesting the higher probability of contraction bursts
372 and pulses was in fact due to mechanical stimulation (Figure 3 – Figure Supplement 4). Thus,
373 based on the comparison between the probability of spontaneous contraction bursts and pulses
374 and mechanosensory response in all resections, we found that the “body column” animals had a
375 weak response to touch despite their slightly increased contraction bursts and pulses probability
376 with mechanical stimulation.
377
378
379 **Oral and aboral networks show different patterns of activity during spontaneous**
380 **contractions compared to mechanically stimulated contractions**
381
382 To identify how the activity of neurons in the oral and aboral networks coordinate spontaneous
383 and stimulated responses, we manually tracked the calcium activity of several neurons in the
384 oral and aboral regions (20 minutes no stimulation, 10 minutes stimulation 1 sec every 31 sec, n
385 = 3 *Hydra*; (Figure 4a, b, Figure 4 – Figure Supplement 1 and 2). We found there were at least
386 two independent networks of neurons based on a correlation analysis (Figure 4c). Specifically,

387 we time-aligned the calcium activity with either spontaneous contractions or mechanical
388 stimulation events to classify these groups of neurons based on their activity (Figure. 4d, e, g).
389 One group of correlated neurons found throughout the entire body showed averaged calcium
390 activity less than one second after a mechanical stimulus and spontaneous activity that is
391 consistent with previously reported Contraction Burst (CB) neurons[30]. We plot calcium dynamics
392 of these CB neurons as shades of blue in Figure. 4 (and Figure 4 - Figure Supplement 1 and 2).
393 These neurons show bursts of activity that are synchronized with muscle contractions and show
394 calcium activity that is highly correlated with the average peduncle ROI. In addition to these CB
395 neurons, we found other groups of correlated neurons with average calcium activity that is
396 independent of the CB network. One group showed a distinctive pattern of activity following
397 mechanical stimulation, but no distinctive activity associated with spontaneous contractions.
398 Specifically, this group of neurons near the oral end responded approximately 10 seconds after
399 mechanical stimulation (Figure. 4e, g). We found these putative "mechanically responsive (MR)
400 neurons" in all three *Hydra* we analyzed and plot their calcium dynamics as shades of red in
401 Figure. 4 (and Figure 4 - Figure Supplement 1 and 2). The fact that these MR neurons do not
402 show activity associated with spontaneous contractions clearly indicates that they are not a part
403 of the CB network, but rather these two distinct networks (CB and MR) are involved in the
404 *Hydra's* response to mechanical stimulation. We also note that these MR neurons do not fire
405 periodically as would be expected for the Rhythmic Potential (RP) network[30]. In addition to CB
406 and MR neurons, in *Hydra* 2 (Figure 4 - Figure Supplement 1) and 3 (Figure 4 - Figure
407 Supplement 2) we also found neurons that were not associated with either the MR network or
408 the CB network. These neurons we labeled as "unspecified groups" do not appear to be a part
409 of the CB or RP networks previously characterized nor the MR neurons we identify here.
410
411 These data suggest that there are at least two separate pathways involved in the
412 mechanosensory response. The first involves the CB neurons and muscle contractions. The

413 second network involving the MR neurons responds more slowly, with a latency of several
414 seconds. Because the activity of the MR neurons occurs after the contraction, their role in the
415 behavioral response remains unclear.
416
417
418 ## Discussion
419
420 Our experiments with “footless”, “headless”, “bisected”, and “body column” animals show that
421 mechanosensory and spontaneous behaviors are regulated by neural ensembles that are
422 localized to select regions of the animal; however, some properties of the mechanosensory
423 response may be evenly distributed throughout the body. We demonstrate that localized touch
424 produces an increased calcium activity in both peduncle neurons (Figure 2) and ectodermal
425 epitheliomuscular cells (Figure 3), which is associated with body contractions (Figure 2 - Figure
426 Supplement 4)[31]. We identified at least two neuronal networks (MR and CB network) with
427 distinct neuronal activities mediating the stimulated responses (Figure 4), where the CB network
428 of neurons show fast calcium responses, and the MR neurons show slower calcium response. It
429 is possible that the MR neurons, primarily found in the oral end (N = 3 *Hydra*), may consist of
430 ec4 neurons, which are the only neuronal subtype in the oral end with an unknown function. The
431 other orally located ectodermal neuron populations, ec1B and ec3C, are suggested to belong to
432 the CB and RP1 circuits, respectively[48]. *Hydra’s* responsiveness (i.e., probability of response to
433 a mechanical stimuli) depends on the stimulus intensity (Figure 2). Interestingly, we found that
434 the “headless” and “footless” animals can still respond to mechanical stimuli despite missing an
435 entire regional neuronal network; however, “headless” animals show reduced responsiveness
436 (Figure 3 and Figure 3 - Figure Supplement 3). The “body column” animals missing both
437 regional neuronal networks have the most dramatically reduced responsiveness, suggesting

438 that these two neuronal networks work together and play compensatory roles in mediating the
439 mechanosensory response.
440
441 Surprisingly, although the activity of the peduncle nerve ring is strongly associated with
442 spontaneous contractions, these neurons are not necessary for body contraction and response
443 to mechanical stimulation. This raises the question of what role the peduncle nerve ring plays in
444 *Hydra* behavior. One possible explanation is that this nerve ring coordinates body contractions
445 by enhancing the neural signal to ectodermal cells. An additional 4-second reduction in body
446 contraction duration in “body column” animals compared to headless animals supports the idea
447 that the peduncle nerve ring is also involved in coordination of contractile behavior (Figure 3 –
448 Figure Supplement 5). Furthermore, calcium activity propagates from the foot to the hypostome
449 in whole animals during body contractions[70], supporting a hypothesis that the peduncle network
450 of neurons may be motor neurons.
451
452 Based on these observations, we propose a simple model for sensorimotor information flow in
453 *Hydra* where we consider the hypostome as an integration point where sensory and motor
454 information converge. The information is then communicated to the peduncle where it is
455 amplified for coordinated whole body control. There may be sufficient functional redundancy
456 between the hypostome and peduncle regions such that removal or damage to one of them is
457 well tolerated in *Hydra*. Moreover, the diffuse network in the body column may retain minimal
458 processing capabilities needed for weak sensorimotor responses. The fast and slow calcium
459 responses from the CB and MR neurons, respectively, indeed support the hypothesis that *Hydra*
460 have multiple, separate pathways for behavioral response.
461
462 Overall, the quantitative characterization of *Hydra’s* sensorimotor responses reported here help
463 to build the foundation for a more comprehensive investigation of information processing in

464 *Hydra*—an animal with clear advantages to supplement commonly studied model organisms in
465 neuroscience. Important next steps include developing mechanistic models to describe sensory
466 information processing that supports our results. Although our experiments describe general
467 information flow in *Hydra*, having a cellular level control of neuronal activity would be a clear
468 advantage for revealing the function of neuronal cell types as well as their functional
469 connectivity in the sensorimotor circuits. We expect additional future work with optogenetic
470 manipulation of specific neuronal subtypes combined with fast, volumetric and ratiometric
471 imaging techniques will provide a more comprehensive approach for characterizing this
472 sensorimotor processing in *Hydra*. Recognizing that calcium fluorescence imaging is limited in
473 its ability measure single spikes[71], we also expect other activity sensors (such as voltage
474 indicators) will reveal what role the MR neurons play in behavioral response. Building upon the
475 work reported here, one can then interrogate the roles of these regional networks with multiple
476 sensory modalities, such as light and heat, to answer questions about how diffuse nervous
477 systems may be capable of centralized information processing and multisensory integration.
478 These studies may help reveal a comprehensive model for how internal states and external
479 stimuli shape the behavioral repertoire in an organism with a highly dynamic neural architecture.
480
481

482 Materials and Methods

483

484 *Hydra* strains and maintenance

485

486 *Hydra* were raised in *Hydra* medium at 18°C in a light-cycled (12 hr: 12 hr; light: dark) incubator
487 and fed with an excess of freshly hatched *Artemia nauplii* (Brine Shrimp Direct, Ogden, UT,

488 #BSEP8Z) three times a week (protocol adapted from Steele lab). All experiments were
489 performed at room temperature with animals starved for 2 days.
490
491 The transgenic line nGreen, kindly provided by Rob Steele, was generated by microinjecting
492 embryos with a plasmid containing the *Hydra* actin promoter driving GFP expression[48]. The
493 transgenic strains expressing GCaMP6s under the actin promoter in neurons and in ectodermal
494 epitheliomuscles (Addgene plasmid: #102558) were developed by microinjections of the
495 embryos by Christophe Dupre in the Yuste lab (Columbia University)[57]. The transgenic strain
496 expressing GCaMP7b in ectodermal epitheliomuscular cells was co-developed by Juliano Lab
497 (University of California, Davis) and Robinson Lab (Rice University). Briefly, the plasmid with
498 codon optimized GCaMP7b under the EF1a promoter was constructed by GenScript
499 (www.GenScript.com). Injections were performed as previously described[72] with the following
500 modifications: 1) injection solution was prepared by mixing 1 µL 0.5% phenol red (Sigma P0290-
501 100ML) with 6 µL plasmid DNA solution prior to centrifugation, and 2) embryos were fertilized
502 for 1-2 hours prior to injection. Plasmid promoters were cloned in expression vector pHyVec2
503 (Addgene plasmid: # 34790) using restriction sites NsiI. Plasmids were prepared by Maxiprep
504 (Qiagen, Valencia, CA) and eluted in RNase-free water. A plasmid DNA solution of 1.4 µg/uL
505 was injected into embryos using an Eppendorf FemtoJet 4x and Eppendorf InjectMan NI 2
506 microinjector (Eppendorf; Hamburg, Germany) under a Leica M165 C scope (Leica
507 Microscopes, Inc; Buffalo Grove, Il). Viable hatchlings with mosaic expression were propagated
508 by asexual reproduction, and asexual buds were screened and selected for increasing amounts
509 of transgenic tissue until a line was established with uniform expression in the ectodermal
510 epithelial cells.
511
512 **Fluorescence imaging of *Hydra* nerve net**
513

514 Distribution of neurons in the *Hydra* nerve net was fluorescently imaged with transgenic *Hydra*
515 *vulgaris* expressing GFP (nGreen) in neurons and neuronal progenitors (Figure 1a)[48]. *Hydra*
516 was anesthetized with 0.05% chloretone and immobilized in a ~160 μm tall microfluidic
517 chamber[31]. High-resolution fluorescence imaging was performed using a confocal microscope
518 (Nikon TI Eclipse) and 10x (0.45NA) objective, where the *Hydra* was imaged at a single plane
519 with multiple fields of views stitched together to obtain an image of the whole animal (Figure 1a).
520
521 ***Hydra* resections**
522
523 *Hydra* were placed in a petri dish and covered with enough *Hydra* medium to prevent
524 desiccation. When *Hydra* were relaxed and stationary, resections were performed with a single
525 incision with a scalpel across the body. We referenced published images of in-situ
526 hybridizations of different cell types and spatial expression patterns to guide the location of
527 incisions. For "footless" *Hydra,* an axial cut above the peduncle removed ~one third of the lower
528 body, which included the peduncle and the basal disk. For "headless" *Hydra,* an axial cut below
529 the hypostome removed ~one third of the upper body, including the tentacles and the
530 hypostome. For "bisected" *Hydra*, a transverse cut starting from the tip of the hypostome to the
531 basal disk was made along the midline of the body. For "body column" *Hydra*, an axial cut
532 above the peduncle removed the lower body followed by another axial cut below the hypostome
533 to remove the upper body region. This preparation resulted in an open tube body. *Hydra* were
534 stored in an 18°C incubator after the excisions and until beginning the experiments. *Hydra* can
535 seal open wounds within ~3-4 hours and repopulate the neuronal population to regain
536 functionality in 30-72 hours (Figure 3 – Figure Supplement 1, see "Imaging regeneration of
537 peduncle network"). To allow *Hydra* time to recover but not regain the functionality of lost
538 neuronal cell types, we performed experiments 6-12 hours post amputation.
539

540 **Imaging regeneration of peduncle network**
541

542 Transgenic *Hydra* (GcaMP6s, neurons) were axially cut in the middle of the body column to
543 generate an oral and aboral halves (Figure 3 – Figure Supplement 1a). The oral half was
544 immobilized between two coverslips with a ~110 μm PDMS spacer. Calcium fluorescence was
545 conducted for 20 min every 2 hr on Nikon TI Eclipse inverted microscope with 20% excitation
546 light from Sola engine and GFP filter cube. We captured frames at ~10Hz (100ms exposures)
547 with Andor Zyla 4.2 sCMOS camera with NIS software. We used 4x (0.2 N.A) objective for wide-
548 field imaging to fit the entire *Hydra* in the field of view reduce the likelihood of *Hydra* migrating
549 out of the imaging frame. *Hydra* were exposed to blue excitation light for 20 min during imaging
550 and remained under dark conditions for 100 min between subsequent imaging timepoints. One
551 animal was imaged for ~20 hours starting with 1 hr post resection (Figure 3 – Figure
552 Supplement 1b). *Hydra* had a visibly open wound at the first imaging point but was not
553 detectable after 3 hr. There were no visibly active neurons in the regenerating aboral end,
554 indicating that the resected peduncle neurons had not regenerated. Another animal was imaged
555 for ~30 hours starting with 37 hr post resection (Figure 3 – Figure Supplement 1c). At the first
556 imaging time point (t = 37 hr post resection), there were few neurons in the peduncle region that
557 were active during body contractions, and these groups of neurons resembled a nerve ring as
558 early as 41 hr post resection. Although the peduncle nerve ring seemed to have formed at this
559 point, it appeared to not be as densely populated qualitatively as observed in whole animals.
560

561 **Microfluidic device fabrication**

562

563 The mechanical stimulation devices are double-layer microfluidic devices with push down valves
564 custom-designed with CAD software (L-edit) and fabricated using standard photo- and soft-
565 lithography techniques. All master molds were fabricated with transparency photomasks and

566 SU-8 2075 (MicroChem). The master mold for the bottom *Hydra* layer (circular chambers, 3 mm
567 diameter) was fabricated with the height of ~ 105-110 μm thick pattern (photoresist spun at
568 300rpm for 20 sec, 2100 rpm for 30 sec). The master mold for the top valve layer (9 individual
569 circular valves, 3 x 3 arrangement, 400 μm diameter each) was fabricated with height of ~110
570 μm thick (photoresist spun at 300rpm for 20sec, 2100 rpm for 30 sec). Polydimethylsiloxane
571 (PDMS) Sylgard 184 was used to cast microfluidic devices from the master molds. The bottom
572 *Hydra* layer (10:1 PDMS spun at 300rpm for 40 sec ~3 hr post mixing; cured for 12 min at 60°C)
573 was bonded to the valve layer (~4 mm thick, 10:1 PDMS; cured for ~40 min at 60°C with holes
574 punched for inlet ports) with oxygen plasma treatment (Harrick Plasma, 330 mTorr for 30 sec)
575 and baked for at least 10 min at 60°C. *Hydra* Insertion ports were hole-punched through the two
576 layers for *Hydra* layer with 1.5 mm biopsy punches, and the devices were permanently bonded
577 (O2 plasma treatment, 330 mTorr for 30 sec) to 500 μm thick fused silica wafer (University
578 Wafers) and baked for at least 1 hr at 60°C. The design files for the photomasks and step-by-
579 step fabrication protocols will be available on www.open*Hydra*.org (under Resource
580 hub/Microfluidics).
581
582 *Hydra* were immobilized and removed from the microfluidic device using syringes to apply
583 alternating positive and negative pressures as previously reported[31]. The microfluidic devices
584 were reused after cleaning similarly to the protocol previously reported. Briefly, the devices were
585 flushed with deionized water, sonicated (at least 10 min), boiled in deionized water (160°C for 1
586 hr), and oven dried overnight.
587
588 After repeated use, the PDMS stiffness can change and affect the valve deflection and the
589 actual force experienced by *Hydra* through the PDMS membrane. Additionally, uncontrollable
590 conditions during the device fabrication process can also lead to small differences between
591 devices. As a result, all data for Figure 2 was taken with a single device and the response curve

592 was used to calibrate (identify pressure that yielded ~ 60% response probability equivalent to
593 20-22 psi stimulus intensity) new devices.
594
595 **Microfluidic mechanical stimulation**
596
597 We used compressed air to inflate the microfluidic valves. For temporal control over valve
598 (on/off) dynamics, we used a USB-based controller for 24 solenoid pneumatic valves (Rafael
599 Gómez-Sjöberg, Microfluidics Lab, Lawrence Berkeley National Laboratory, Berkeley, CA
600 94720) and a custom-built Matlab GUI (available at www.open*Hydra*.org) that allowed setting
601 the stimulation parameters, such as the duration of valve 'on' (1 sec), duration of valve 'off' (30
602 sec), and the duration of stimulation (60 min, 119 cycles of valve 'on' and 'off'), and pre, post-
603 stimulation acclimation/control period (20 min). We used a pressure regulator to manually
604 control the air pressure into the valve manifold. In summary, we set the stimulation pressure
605 with a pressure gauge to regulate the flow of air into the valve manifold. This valve manifold was
606 controlled with a USB valve controller that allowed us to programmatically inflate the valve (turn
607 it 'on') with pressurized air with custom stimulation parameters.
608
609 To test sensory motor response to mechanical stimuli, we used pressurized air to inflate the
610 push-down valve and cause it to press down on the *Hydra* immobilized in the bottom layer.
611 Each experimental condition had at least three *Hydra* each. For a given condition, replication
612 experiments were conducted on different days. After an animal was immobilized inside the
613 *Hydra* chamber, we selected one valve (from the nine valves over the entire chamber) that was
614 directly above the mid-body column region to deliver stimuli. Although *Hydra* were free to move,
615 we did not observe large displacement most of the time and, as a result, the same valve
616 remained in contact with the animal throughout the stimulation period.
617

618 We adjusted the air pressure using a pressure regulator for each experiment, and the valves
619 were inflated using a USB valve controller (see above). The full-length stimulation experiment
620 consisted of 20 min of no stimulation (control/acclimation) followed by 60 min of stimulation
621 period (except habituation experiment where the stimulation period was 120 min), where valves
622 were pulsed with constant pressure (0 (control), 5, 10, 15, 20, 22 or 25 psi) for 1 sec every 31
623 sec, then another 20 min of no stimulation (control/acclimation). Shorter stimulation experiment
624 (used for whole-animal muscle imaging of various resections) consisted of 20 min of no
625 stimulation (acclimation/control) followed by 20 min of stimulation period (valves pulsed for 1
626 sec every 31 sec with a constant pressure of 0 or 22psi). We chose a 20 min initial control
627 period based on the high sensitivity to abrupt changes in light intensities (especially to blue
628 wavelengths used for excitation of GCaMP) in *Hydra* which leads to increased contractile
629 activity for 2-5 min. Even with the stimulus repeated for two hours at a constant inter-stimulus
630 interval, we found no obvious evidence of sensitization, habituation, or stimulus entrainment in
631 *Hydra* (Figure 2 – Figure Supplement 9). As a result, we chose not to randomize the inter-
632 stimulus interval.
633
634 **Distribution of mechanical forces**
635
636 We characterized the distribution of force exerted by a microfluidic valve by quantifying the
637 movements of neurons due to mechanical stimulation. We performed fluorescence imaging in
638 transgenic *Hydra* (nGreen) expressing GFP in neurons for ~8 min. We captured 8,000 frames at
639 ~16Hz (50 msec exposures) with 4x objective (0.2 N.A.) and Andor Zyla 4.2 sCMOS camera
640 with 2x2 binning (1024x1024 frame size) using MicroManager. *Hydra* was stimulated in the
641 middle of the body column (valve pulsed for 1 sec every 31 sec, 5 times).
642

643 To quantify the movement of neurons and tissue throughout the *Hydra* body, we tracked a total
644 of 222 neurons that were visible for 1 min capturing the first two stimulation trials. We performed
645 semi-automated tracking with TrackMate plugin (ImageJ/(Fiji)[72–74]and manually corrected the
646 tracks where neurons were misidentified. From these tracks, we calculated the displacement of
647 each of the neurons between each frame (~50 msec). The average cellular displacement (0.4
648 μm per frame, 50 msec) was calculated by averaging the cellular displacements from all frames
649 when the valve was not pressurized. We found a significantly increased displacement (6.2 um, p
650 < 0.001) just after the valve was pressurized (and after the valve was depressurized 1 sec
651 later). We then generated a vector map of neuronal displacements by calculating the change in
652 position of each of the neurons in the frame just after the valve was pressurized for the first
653 stimulation trial (Figure 2 - Figure Supplement 1a). We also plotted the cellular displacement for
654 each of the neurons and the location of those neurons relative to the center of the valve. We
655 averaged the highest three displacements in 50 μm radial band increments from the valve
656 center to quantify how far the mechanical forces extended. This was a more conservative
657 measurement as the neurons in different tissue layers (endodermal and ectodermal layers
658 furthest from the valve) may have experienced different forces. By taking the average of the
659 highest three displacements in 50 μm radial bands increments from the valve center, we
660 identified the majority of the (shear) force was experienced by neurons bordering the valve in
661 250 μm radius.
662

663 **Fluorescence intensity from GFP *Hydra***
664

665 To prove that the fluorescence intensity changes we observed with calcium imaging are due to
666 calcium activity and not motion artifacts from body contractions, we compared the average
667 fluorescence intensities from three different transgenic *Hydra* lines: 1) expressing GFP pan-
668 neuronally (nGreen line), 2) expressing GCaMP6s pan-neuronally, and 3) expressing GCaMP7b

669 in ectodermal epitheliomuscular cells (Figure 2 - Figure Supplement 3). For each *Hydra*, we
670 compared the average fluorescence intensities from three different regions of interest (ROIs)
671 that included the peduncle region, whole frame (for whole body) region, and valve region. We
672 also measured the body length by taking the major axis of an ellipse fitted along the oral-aboral
673 axis of the body column (from apex of the hypostome to the basal disc) after binarizing the
674 fluorescence image.
675
676 For this analysis, we used fluorescence imaging from transgenic *Hydra* expressing GFP pan-
677 neuronally (nGreen) performed in "Distribution of mechanical forces". *Hydra* was stimulated in
678 the middle of the body column (valve pulsed for 1 sec every 31 sec, 5 times). We used calcium
679 imaging from transgenic *Hydra* (expressing either GCaMP6s pan-neuronally or GCaMP7b in
680 ectodermal epitheliomuscular cells) stimulated in the middle of the body column (valve pulsed
681 for 1 sec every 31 sec, 120 times). The average fluorescence intensity and body length traces
682 were time-aligned to the onset of mechanical stimulation to show 1) changes in average
683 fluorescence intensity in peduncle ROI and the whole frame ROI are due to calcium activity
684 (increase in fluorescence from in GCaMP lines) and not motion artifact (no change in
685 fluorescence from GFP line) and 2) increase or decrease in body length or average
686 fluorescence from valve ROI are affected by stimulation artifacts.
687
688 **Average calcium fluorescence from large and small ROIs in the peduncle**
689
690 We performed fluorescence imaging in transgenic *Hydra* expressing GCaMP6s in neurons for
691 ~1 min during spontaneous behaviors (*Hydra* was not stimulated). We captured frames at
692 ~16Hz (50 msec exposures) with a 10x objective (0.45 N.A.) and Andor Zyla 4.2 sCMOS
693 camera with 3x3 binning (682x682 frame size) using MicroManager.
694

695 Because calcium fluorescence decreases when neurons are inactive, tracking multiple neurons
696 in a highly deformable region is a challenge. Nonetheless, we tracked 9 neurons from the
697 peduncle nerve ring that were visible (enough to track) for 1 min. We performed semi-
698 automated tracking with TrackMate plugin (ImageJ/(Fiji)[72–74] and manually corrected the tracks
699 where neurons were misidentified. We also used a large peduncle ROI, similar to how we used
700 an ROI for quantifying neural response to stimulation in all other experiments. We calculated the
701 average calcium fluorescence trace from small ROIs for individual neurons and large ROI for
702 the peduncle region. Fluorescence intensity was normalized by calculating $\Delta F/F$, where $\Delta F = F-$
703 F_0 and F_0 is the minimum fluorescence from prior time points. The large peduncle ROI had
704 highly correlated calcium fluorescence activity with smaller ROIs for individual neurons which
705 are known to belong to the contraction burst circuit (Figure 2 - Figure Supplement 2). As a
706 result, for all other experiments we use large peduncle ROI when measuring the neuronal
707 activity.
708
709 **Whole-animal imaging of neural activity at different stimulus intensities**
710
711 We characterized the neural response to repeated local mechanical stimuli at 0 (control), 5, 10,
712 15, 20 and 25 psi pressure with animals that expressed GCaMP6s in neurons (Figure 2). Each
713 pressure condition was experimented with three animals on different days using the same
714 device and stimulation protocol (valve pulsed for 1 sec every 31 sec for 60 min) to generate the
715 pressure-response curves (total of 18 animals). Calcium fluorescence imaging for all
716 experiments was conducted for the 100 min duration of the stimulation protocol (see Mechanical
717 Stimulation subsection) on Nikon TI Eclipse inverted microscope with 20% excitation light from
718 Sola engine and GFP filter cube. We captured 100,000 frames at ~16Hz (50 msec exposures)
719 with Andor Zyla 4.2 sCMOS camera with 4x4 binning using MicroManager. For imaging neural
720 activity, 12-bit low noise camera dynamic range was used. To synchronize the stimulation onset

721 times with imaging, we use used a data acquisition device (LabJack U3) to record the TTL
722 frame out signal (fire-any, pin #2) from the Zyla and the valve on/off timestamps from the valve
723 controller.
724
725 We used 4x (0.2 N.A.) objective for wide-field imaging to fit the entire *Hydra* in the field of view
726 to reduce the likelihood of *Hydra* migrating out of the imaging frame. There are neurons in the
727 oral region (hypostome) that are co-active with aboral region (peduncle) neurons during body
728 contractions; however, neurons in the hypostome appeared to be much sparser than those in
729 peduncle (Video 18). Discerning these hypostomal network neurons required higher
730 magnification which significantly reduced the field of view such that considerable amount of
731 nervous tissue could move in and out of the imaging plane (z-plane) or frame (xy-plane), making
732 it difficult to obtain reliable calcium fluorescence time-series.
733
734 **Whole-animal imaging of neural activity with different stimulation regions**
735
736 To map the sensitivity of different body parts to mechanical stimuli, we performed calcium
737 imaging of multiple animals (N = 3, whole animals expressing GCaMP6s in neurons) using
738 imaging settings previously described with modified experimental protocol. Based on the range
739 animal sizes (1-2.5 mm) and the size of the valve (400 um), we stimulated *Hydra* body at three
740 different regions along the oral-aboral axis: 1) the oral end (upper third of the body), 2) the
741 aboral end (lower third of the body), and 3) the third near the mid-body column. Each animal
742 was stimulated at three different locations (20 min no stimulation, stimulation region #1 - 1 sec
743 every 31 sec for 20 min, ~2 min no stimulation, stimulation region #2 - 1 sec every 31 sec for 20
744 min, ~2 min no stimulation, stimulation region #3 - 1 sec every 31 sec for 20 min using 22 psi).
745 We randomized the order in which the three different body regions were stimulated in each of
746 the three animals to avoid any stimulus entrainment artifacts. We then analyzed the peduncle

747 nerve ring activity in response to mechanical stimulation of different body regions as details in
748 “Analysis of calcium activity” and “Analysis of mechanosensory response”.
749
750 **Whole-animal imaging of neural activity in resected animals**
751
752 For experiments that involved body lesions (Figure 3 – Figure Supplement 3), the same
753 experiment protocol and imaging settings as previously described (see “whole animal imaging of
754 neural activity at different stimulus intensities”, 20 min no stimulation, stimulation 1 sec every 31
755 sec for 60 min, 20 min no stimulation) were used with either 0 psi (control) or 20 - 22 psi (~ 60%
756 response probability). Each condition group had three animals (total of 18 animals). The
757 “headless” and “bisected” animals were prepared with the appropriate body regions removed as
758 described previously (*“Hydra* resections”). Due to difficulty in tracking neurons and weak
759 GCaMP expression in body column neurons, we were unable to quantify responses from
760 “footless” and “body column” *Hydra* and thus excluded them from experiments.
761
762 **Simultaneous electrophysiology and calcium imaging of ectodermal epitheliomuscular**
763 **cells**
764
765 Electrical activity from the epitheliomuscular cells was measured simultaneously with calcium
766 imaging of the ectodermal epitheliomuscular cells in transgenic *Hydra* using a nano-SPEARs
767 device previously reported (Figure 2 – Figure Supplement 4)[31]. Briefly, transgenic *Hydra*
768 expressing GCaMP6s in the ectodermal epitheliomuscular cells starved for at least 48 hr were
769 used to measure the activity of the muscles (10 fps, 30 min, 4x objective with 15% light
770 intensity). An inverted microscope with GFP filter and Andor Zyla 4.2 were used for capturing
771 images. All electrical data was obtained with an Intan Technologies RHD2132 unipolar input
772 amplifier (http://intantech.com) at a sampling rate of 1KHz, low frequency cutoff and DSP filter of

773 0.1 Hz and high frequency cutoff of 7.5 KHz. From the calcium activity traces, we identified 30
774 sec intervals of either high amplitude activity or low amplitude activity to perform cross-
775 correlation analysis. The high and low amplitude activity regions were manually identified with a
776 threshold of 20% of the highest peak in the calcium activity. The high amplitude activity region
777 occurred during contraction bursts. The low amplitude activity region occurred during tentacle
778 contractions for muscular activity imaging. Both the Intan amplifier and the Zyla were triggered
779 with the same TTL signal. However, to account for any offset in the timing of the electrical and
780 optical data, we measured the maximum of the cross-correlogram in a 50 ms (approximately
781 one duty cycle of the trigger signal) window rather than the cross-correlation at zero offset to
782 generate the correlation maps. For correlation map, each frame was down sampled to 64 x 64
783 pixels, and the fluorescence trace for the downsampled pixels across the 30 sec intervals was
784 cross-correlated with electrical activity during the same 30 sec interval. The intensity of color in
785 the correlation map was used to indicate correlation values.
786
787 **Whole-animal imaging of epitheliomuscular activity at different stimulus intensities**
788
789 We characterized the muscle response to mechanical stimuli using animals that expressed
790 GCaMP7b under the EF1a promoter in ectodermal epitheliomuscular cells (Figure 3). We
791 measured contraction pulses and contraction bursts by averaging calcium activity in all the
792 epitheliomuscular cells (Figure 3a). The correlation between peduncle nerve ring activity and
793 muscle contractions has been previously established based on simultaneous electrophysiology
794 and neuronal[31] or ectodermal epitheliomuscular cells calcium imaging (Figure 2 – Figure
795 Supplement 4). The imaging protocol for epitheliomuscular cells was similar to the imaging of
796 neural activity (see “whole animal imaging of neural activity at different stimulus intensities”),
797 except a 16-bit camera dynamic range was used to avoid saturating the sensor.
798

799 We first developed a partial psychometric curve for calcium activity of epitheliomuscular cells to
800 confirm the dependence of response on stimulus intensity. Three animals were imaged for 20
801 min without stimulation and then stimulated at three different pressures (20 min at 15psi, 20 min
802 at 20 psi, 20 min at 25psi; or in reverse order), and the epitheliomuscular response curve was
803 used to identify the stimulus intensity (~ 22psi) which yielded ~ 60% response probability
804 (Figure 2 - Figure Supplement 5). This stimulation intensity was also selected for stimulation of
805 N = 8 whole animals (40 min of imaging; 20 min of no stimulation, 20 of stim for 1 sec every 31
806 sec with 22 psi) and animals with different body regions removed.
807
808 **Whole-animal imaging of epitheliomuscular activity in resected animals**
809
810 The various body regions were removed as described previously (*"Hydra* resections") to
811 prepare "headless", "footless", "bisected" and "body column" *Hydra*. Note, this transgenic line of
812 *Hydra* expressing GCaMP7b in the ectodermal cells showed some signs of deficit. They were
813 particularly sensitive to being handled and were more likely to dissociate after ~30 min in the
814 chambers during long-term microfluidic immobilization and fluorescence imaging. The resected
815 *Hydra* were especially difficult to image for the entire 100 min without any cell dissociation. This
816 could be due to the specific promoter used for driving GCaMP expression or that phototoxicity is
817 higher when there is a high expression of GCaMP in a larger number of cells. Because the
818 lesioned animals were more likely to be damaged during microfluidic immobilization, the
819 mechanical stimulation protocol (see Mechanical Stimulation subsection) was shortened to total
820 of 40 min of imaging with 20 min of no stimulation followed by 20 min of repeated stimulation (1
821 sec every 31 sec for 20 min). For three animals per each resection (total of 30 animals), we
822 used the full-length protocol (100 min of imaging: 20 min of no stimulation, 60 min of stimulation
823 every 31 sec, and 20 min of no stimulation) to obtain higher statistical power for quantifying
824 response probability (Figure 3 – Figure supplement 3). A total of 6-8 animals were stimulated for

825 each resection condition (whole, N = 6 not-stimulated, N = 8 stimulated; “footless”, N = 4, not-
826 stimulated, N = 8 stimulated; “headless”, N = 5 not-stimulated, N = 8 stimulated; “bisected”, N =
827 5 not-stimulated, N = 8 stimulated; “body column” N = 3 stimulated, N = 6 stimulated; total 61
828 animals, Figure 3; 30 of which were experimented with long (100 min) stimulation protocol
829 Figure 3 – Figure supplement 3).
830

831 **Analysis of calcium activity**
832

833 To analyze neural response, we used the average fluorescence from the peduncle region.
834 Tracking individual neural responses was difficult due to high deformability of the body and lack
835 of fluorescence markers when neurons were not active; as a result, we looked at the
836 synchronous firing activity of the neurons in the peduncle region, which is known to have high
837 correlation with body contractions. To analyze epitheliomuscular response, we used average
838 fluorescence from the whole animal to obtain the fluorescence signal over time and analyzed
839 these signals similarly to neural response. Briefly, using ImageJ (Fiji)[72,73] we used a ROI over
840 the peduncle region or the whole *Hydra* to obtain fluorescence signal over time for neuronal or
841 epitheliomuscular calcium activity, respectively.
842

843 From the fluorescence signal, we detected the large calcium spikes as individual contractions
844 (contraction pulses or bursts) using MATLAB peak finding algorithm. We generated a raster plot
845 of calcium spiking activity time-aligned with the stimulus where each row represented one
846 stimulation trial with 15 sec before and after stimulation onset. These raster plots were used to
847 calculate the probability for spontaneous contraction and mechanosensory response.
848 For contractile behavior analysis, we then annotated the calcium spikes. Single calcium spikes
849 were labeled as single pulse contraction. A volley of calcium spikes was labeled as a
850 contraction burst. Both of these led to behavioral contractions, thus time between contractions

was calculated as the time between the end of a contraction event (single pulse or burst) and the start of the next one (as shown in Figure 3 – Figure Supplement 5). Percent of contractions that are single pulse contractions was calculated as the fraction behavioral contractions that were single calcium spikes (not bursts). Contraction duration was used to indicate the amount of time contraction behavior lasted (time from rise in fluorescence signal to return to baseline, as shown in Figure 3 – Figure Supplement 5)

Analysis of mechanosensory response

To obtain the response probability (whether an animal had a contraction pulse—either a single pulse or a pulse from a burst) at the time of stimulation (when valve was pressurized), we generated a raster plot of fluorescence spikes time-aligned to stimulus onset and superimposed for each 30 sec intervals (time between stimulus). We used an hour of activity (t = 20-80 min) to generate the raster plot and calculate response probability. We defined the 1 sec window while the valve was pressed as the response window for each trial (Figure 2 – Figure Supplement 6). We then calculated the fraction of all trials (119 trials over 60 min or 40 trials over 20 min) per animal that had at least one fluorescence spike ("contraction pulse") in the 1 sec response window following stimulus onset to obtain the contraction probability. Extraction of raw fluorescence for ROIs was performed with ImageJ (Fiji)[72,73] and post-processing analysis was performed with MATLAB (using peak-finding algorithm to detect spikes). A one-way ANOVA with Bonferroni correction was used for statistical analysis.

For animals with shorter experiment duration, the mechanosensory response probability in stimulated animals was calculated over the 20 min segment (time = 20-40 min) with a fraction of all trials (40 trials over 20 min) that had at least one fluorescence spike. A one-way ANOVA with Bonferroni correction was used for statistical analysis when comparing multiple conditions. A

877 paired t-test was used to compare the difference between probability of spontaneous
878 contraction and mechanosensory probability in the same animals for each of the conditions. The
879 effect size (magnitude of difference) was measured with Cohen's d and Cliff's delta.
880

881 **Analysis of spontaneous contraction**
882

883 For non-stimulated animals, fluorescence activity from one hour of activity (time = 20-80 min)
884 was converted into a raster plot with multiple (119 trials over 60 min) 30 sec long intervals (to
885 match the stimulation interval in stimulated animals). We obtained "stimulation times" using a
886 DAQ to record the signal from valve controller except the air pressure was set to 0 psi. The
887 spontaneous contraction probability was calculated by taking the average of response
888 probability from a random 1 sec interval (Figure 3 and Figure 3 – Figure Supplement 3). Briefly,
889 by sliding a 1 sec window by ~0.3 sec over the x axis (30 sec of stimulation interval) on the
890 raster plot (pooled from all three animals for Figure 4a, per individual stimulated animal for
891 Figure 3 – Figure Supplement 3), we generated the distribution of the fraction of trials (119 trials
892 x 3 animals over 60 min) with at least one contraction event in a random 1 sec response window
893 (Figure 3 – Figure Supplement 3). The distributions were compared with a Kruskal-Wallis test.
894

895 For animals with shorter experiment duration, spontaneous contraction probability in stimulated
896 animals was calculated similar to non-stimulated animals above, except the raster plot was
897 generated with the first 20 min of fluorescence activity (time = 0-20 min) when no stimulation
898 was applied. Briefly, we generated a distribution of random probabilities by sliding a 1 sec
899 window over the x-axis on the raster plot and used the distribution mean as the spontaneous
900 contraction probability to compare with mechanosensory response probability from the same
901 animal with a paired t-test (Figure 3). For non-stimulated animals with shorter experiment
902 duration, spontaneous contraction probability was also calculated over the second 20 min

903 interval (t = 20-40 min) to confirm the increase in contraction probability during mechanical
904 stimulation was in fact due to stimuli and not just from temporal variation in spontaneous
905 contractions (Figure 3 – Figure Supplement 4). Note, these experiments were performed with
906 *Hydra* constrained to ~110um thick microfluidic chambers. Although animals are able to behave
907 under such confinements, the range of behavioral motifs and rates may be altered due to
908 compression.
909

910 **Neuron subtype gene expression analysis with RT-qPCR**
911

912 Resected *Hydra* were prepared as described above, with 12 polyps per biological replicate
913 (except 6 whole polyps for control) and a total of two biological replicates per treatment.
914 Approximately 12 hrs post resections, tissue was frozen in 1 mL Trizol at -80°C until use. RNA
915 was isolated using the Zymogen RNA Clean and Concentrator kit (Zymogen #R1017) with an
916 in-column Zymogen DNAse I digestion (Zymogen #E1010) following the manufacturer's
917 protocol. cDNA was synthesized using 1 µg of purified RNA and Promega M-MLV RNase H
918 Minus Point Mutant Reverse Transcriptase (Promega, Madison, WI M3682) using the
919 manufacturer's protocol for oligo dT-primed synthesis. cDNA synthesis was validated via PCR,
920 and all cDNA samples were diluted 1:10 in nuclease-free water for use in qPCR experiments.
921

922 Each sample was run in three technical replicates per gene in a 10 uL qPCR reaction using Bio-
923 Rad SsoAdvanced universal SYBR green master mix (Bio-Rad, Hercules, CA 1725271).
924 Samples were run on a CFX96 Touch Real-Time PCR Detection System (Bio-Rad 1855195).
925 Data were analyzed with the $2^{-\Delta\Delta Ct}$ method using the 'tidyverse' package in R[75,76].
926

927 Briefly, Cq values from technical replicates were pooled for subsequent analyses. *rp49* was
928 used as an internal control to calculate ΔCq values after first being found to give similar results

929 across all treatments when compared to a second control gene, *actin.* All results were
930 normalized to the "whole" animal samples. A template-free water control was performed for all
931 primer sets to ensure contamination-free reactions. All qPCR primers (Table 1) were validated
932 via a 10-fold serial dilution standard curve to have a binding efficiency over 90%.
933
934 *Table 1: qPCR primers for neuronal subtypes*

Subtype	transcriptID	F sequence	R sequence
en1	t29955aep	GCC GCA GTA TCA TCA TAC AAA TC	CCA TAA ACC ACA CAT CGC ATA AA
en2	t20666aep	CTT CTT GCT TCT ATC CTC GTT CT	TAC CTC AAG TAA ATT ATC GGT CTC G
en3	t33579aep	CGT TGG TAT GAC TAT AAT CGT TGT TAT G	AGG ATA CAT CAC CCA CCA AAT C
ec1A	t22316aep	GCC TTT CTT TAT CTC GGG TAT CT	ACC TCC CAT GAG TAG CTG TA
ec1B	t20807aep	AAG ATC TAC GAC GTC ATA TCA ATC A	TCA TGC CCT TAT TAC CCT CTT G
ec2	t7411aep	GCG CCT TGT AAC TAT GGT CTT A	TTC GTA GAA CAT TGT CAT CTT CCT
ec3A	t9620aep	CGG TGC TGC TCC TAA TTC AA	CTC CGG TGC ACT GAT TTA TAG G
ec3B	t7664aep	TGT TTC AAA TGC AGA CGA AGA TG	GCG TGT TTA TTT GCC TGG AC
ec3C	t19558aep	CGG TTA GAT ACA CTG CGG TTA G	TAC GTG CCG TTC TTC GTT T
ec4A	t33899aep	GGC TTT AAT CGT TGT AGC TCT TG	CTT GCT ATC TTC TGA CAA GTG ATT G
ec5	t6329aep	CCA ACA ATG GTC GAA TGA AGA AA	ATC GCC AGG TTT GTA TCC TTT A
RP49	t6797aep	GCC AAA CTG GAG AAA ACC TAA AG	TCA GGC ATA AGA TGA CGT GTC
Actin	t11116aep	CGC CCT CGT AGT TGA TAA TGG	AAT CCT TCT GTC CCA TAC CAA C

935
936
937
938 **Whole animal imaging with single neuron resolution**
939
940 We performed fluorescence imaging in transgenic *Hydra (N = 3)* expressing GCaMP6s in
941 neurons for ~30 min (30 min of imaging: 20 min of no stimulation, 10 min of stimulation every 31
942 sec). We captured frames at ~16Hz (50 msec exposures) with a 10x objective (0.45 N.A.) and
943 Andor Zyla 4.2 sCMOS camera with 3x3 binning (682x682 frame size) using MicroManager.
944
945 Because calcium fluorescence intensity is low (almost indiscernible from the autofluorescence
946 of *Hydra*) when neurons are inactive, tracking multiple neurons in a highly deformable region
947 without static nuclear fluorescence (such as RFP) is a challenge. Nonetheless, we manually
948 tracked 5-6 neurons throughout the animal body that were visible (enough baseline
949 fluorescence to track even when the neurons were inactive) for the entire duration of the

imaging. We performed semi-automated tracking with TrackMate plugin (ImageJ/(Fiji)[72–74] to track individual neurons with small circular ROIs (~5 μm radius). We manually tracked (interpolating the current ROI location based on the past and future locations) the neurons when the fluorescence levels were dimmer than the background autofluorescence or when neurons were misidentified by TrackMate. We also used a large peduncle ROI, similar to how we used an ROI for quantifying neural response to stimulation in all other experiments. We calculated the average calcium fluorescence traces from small ROIs for individual neurons and large ROI for the peduncle region. Each of the fluorescence traces were corrected by calculating $\Delta F/F_0$, where F_0 was the mean fluorescence intensity of the trace.

We performed the correlation analysis (MATLAB) of the calcium fluorescence time-series for the individual neuron ROIs and peduncle ROI to identify groups of neurons with correlated activity. We calculated the correlation coefficients for the individual neurons and the peduncle ROI by correlating the entire 30 min calcium fluorescence trace for each of the neurons. These correlation coefficients were shown to be statistically significant then randomly reshuffled calcium fluorescence. We divided each of the neuronal calcium time-series into 30 blocks. These individual blocks were randomly recombined to generate reshuffled time-series for each of the neurons to calculate correlation coefficients. This random reshuffling of each neuron was repeated 1000 times to obtain the mean correlation coefficients for each of the neuron pairs (Figure 4 – Figure Supplement 3d-f). We then calculated the z-score $(x-\mu)/\sigma$, where x is the correlation coefficients of the original raw time-series, μ is the mean correlation coefficients of the time-series randomly reshuffled 1000 times and σ is the standard deviation of the correlation coefficients of the time-series randomly reshuffled (Figure 4 – Figure Supplement 3g-i). To identify the neuronal clusters, we used a hierarchical clustering algorithm (MATLAB function ‘linkage’ with Euclidian distance of correlation coefficients) on the correlation

975 coefficients. We then used leaf order from the linkage tree to sort the neurons and generate the
976 correlation heatmap.
977
978 We calculated the average fluorescence traces from the time-aligned calcium fluorescence to
979 either spontaneous contractions or stimulus events to identify the roles of these neurons. For
980 spontaneous contractions, the calcium fluorescence (t = 0-20 min) was time-aligned to the onset
981 of contraction bursts or pulses from the peduncle ROI. For stimulated contractions, the calcium
982 fluorescence (t = 20-30 min) was time-aligned to the onset of stimulus recorded with a DAQ
983 (see “Whole-animal imaging of neural activity at different stimulus intensities”). We further
984 confirmed the different neuronal clusters identified by performing correlation analysis on all
985 neurons from all three Hydra by calculating the correlation coefficients for the average
986 fluorescence traces from the time-aligned calcium fluorescence to stimulus events (Figure 4f.g).
987

988 ## References

989 1. Clark, D. A., Freifeld, L. & Clandinin, T. R. Mapping and Cracking Sensorimotor Circuits
990 in Genetic Model Organisms. *Neuron* (2013). doi:10.1016/j.neuron.2013.05.006
991 2. Ghosh, D. D., Nitabach, M. N., Zhang, Y. & Harris, G. Multisensory integration in C.
992 elegans. *Current Opinion in Neurobiology* (2017). doi:10.1016/j.conb.2017.01.005
993 3. Kaplan, H. S., Nichols, A. L. A. & Zimmer, M. Sensorimotor integration in Caenorhabditis
994 elegans: A reappraisal towards dynamic and distributed computations. *Philos. Trans. R.*
995 *Soc. B Biol. Sci.* (2018). doi:10.1098/rstb.2017.0371
996 4. Ahrens, M. B. *et al.* Brain-wide neuronal dynamics during motor adaptation in zebrafish.
997 *Nature* (2012). doi:10.1038/nature11057
998 5. Chen, X. *et al.* Brain-wide Organization of Neuronal Activity and Convergent
999 Sensorimotor Transformations in Larval Zebrafish. *Neuron* (2018).
1000 doi:10.1016/j.neuron.2018.09.042
1001 6. Haesemeyer, M., Robson, D. N., Li, J. M., Schier, A. F. & Engert, F. A Brain-wide Circuit
1002 Model of Heat-Evoked Swimming Behavior in Larval Zebrafish. *Neuron* (2018).
1003 doi:10.1016/j.neuron.2018.04.013
1004 7. Hill, A. J., Mansfield, R., Lopez, J. M. N. G., Raizen, D. M. & Buskirk, C. Van. Cellular
1005 Stress Induces a Protective Sleep-like State in C. elegans. *Curr. Biol.* 1–7 (2014).
1006 doi:10.1016/j.cub.2014.08.040
1007 8. Raizen, D. M. *et al.* Lethargus is a Caenorhabditis elegans sleep-like state. *Nature* **451**,
1008 569–72 (2008).
1009 9. Artiushin, G. & Sehgal, A. The Drosophila circuitry of sleep–wake regulation. *Curr. Opin.*
1010 *Neurobiol.* **44**, 243–250 (2017).
1011 10. Guo, F., Holla, M., Díaz, M. M. & Rosbash, M. A Circadian Output Circuit Controls Sleep-
1012 Wake Arousal in Drosophila. *Neuron* **100**, 624-635.e4 (2018).

1013 11. Kayser, M. S. & Biron, D. Sleep and development in genetically tractable model
1014 organisms. *Genetics* (2016). doi:10.1534/genetics.116.189589
1015 12. Gandhi, A. V., Mosser, E. A., Oikonomou, G. & Prober, D. A. Melatonin Is required for the
1016 circadian regulation of sleep. *Neuron* (2015). doi:10.1016/j.neuron.2015.02.016
1017 13. Zhdanova, I. V., Wang, S. Y., Leclair, O. U. & Danilova, N. P. Melatonin promotes sleep-
1018 like state in zebrafish. *Brain Res.* (2001). doi:10.1016/S0006-8993(01)02444-1
1019 14. Zimmerman, J. E., Naidoo, N., Raizen, D. M. & Pack, A. I. Conservation of sleep: insights
1020 from non-mammalian model systems. *Trends in Neurosciences* (2008).
1021 doi:10.1016/j.tins.2008.05.001
1022 15. Kanaya, H. J. *et al.* A sleep-like state in *Hydra* unravels conserved sleep mechanisms
1023 during the evolutionary development of the central nervous system. *Sci. Adv.* **6**,
1024 eabb9415 (2020).
1025 16. Broussard, G. J., Liang, R. & Tian, L. Monitoring activity in neural circuits with genetically
1026 encoded indicators. *Front. Mol. Neurosci.* **7**, 97 (2014).
1027 17. Chen, T.-W. *et al.* Ultrasensitive fluorescent proteins for imaging neuronal activity. *Nature*
1028 **499**, 295–300 (2013).
1029 18. Lemon, W. C. *et al.* Whole-central nervous system functional imaging in larval
1030 Drosophila. *Nat. Commun.* **6**, 7924 (2015).
1031 19. Prevedel, R. *et al.* Simultaneous whole- animal 3D imaging of neuronal activity using
1032 light-field microscopy. *Nat. Methods* **11**, 727–730 (2014).
1033 20. Ahrens, M. B., Orger, M. B., Robson, D. N., Li, J. M. & Keller, P. J. Whole-brain functional
1034 imaging at cellular resolution using light-sheet microscopy. *Nat Methods* **10**, 413–420
1035 (2013).
1036 21. Cong, L. *et al.* Rapid whole brain imaging of neural activity in freely behaving larval
1037 zebrafish (Danio rerio). *Elife* **6**, e28158 (2017).
1038 22. Kim, D. H. *et al.* Pan-neuronal calcium imaging with cellular resolution in freely swimming

1039 zebrafish. *Nat. Methods* **14**, 1107–1114 (2017).
1040 23. Portugues, R., Feierstein, C. E., Engert, F. & Orger, M. B. Whole-brain activity maps
1041 reveal stereotyped, distributed networks for visuomotor behavior. *Neuron* **81**, 1328–1343
1042 (2014).
1043 24. Vladimirov, N. *et al.* Light-sheet functional imaging in fictively behaving zebrafish. *Nat.*
1044 *Methods* **11**, 883 (2014).
1045 25. Gonzales, D. L., Badhiwala, K. N., Avants, B. W. & Robinson, J. T. Bioelectronics for
1046 Millimeter-Sized Model Organisms. *iScience* **23**, 100917 (2020).
1047 26. Nguyen, J. P. *et al.* Whole-brain calcium imaging with cellular resolution in freely
1048 behaving Caenorhabditis elegans. *Proc. Natl. Acad. Sci.* **113**, E1074–E1081 (2016).
1049 27. Nichols, A. L. A., Eichler, T., Latham, R. & Zimmer, M. A global brain state underlies C.
1050 elegans sleep behavior. *Science (80-.).* **356**, eaam6851 (2017).
1051 28. Gonzales, D. L., Zhou, J., Fan, B. & Robinson, J. T. A microfluidic-induced C. elegans
1052 sleep state. *Nat. Commun.* **10**, 1–13 (2019).
1053 29. Aimon, S. *et al. Fast near-whole-brain imaging in adult drosophila during responses to*
1054 *stimuli and behavior*. *PLoS Biology* **17**, (2019).
1055 30. Dupre, C. & Yuste, R. Non-overlapping Neural Networks in Hydra vulgaris.
1056 *Curr. Biol.* **27**, 1085–1097 (2017).
1057 31. Badhiwala, K. N., Gonzales, D. L., Vercosa, D. G., Avants, B. W. & Robinson, J. T.
1058 Microfluidics for electrophysiology, imaging, and behavioral analysis of: Hydra. *Lab Chip*
1059 **18**, 2523–2539 (2018).
1060 32. Bargmann, C. I. & Horvitz, H. R. Chemosensory neurons with overlapping functions direct
1061 chemotaxis to multiple chemicals in C. elegans. *Neuron* **7**, 729–742 (1991).
1062 33. Bargmann, C. I. & Avery, L. Laser Killing of Cells in Caenorhabditis elegans. *Methods*
1063 *Cell Biol.* **48**, 225–250 (1995).
1064 34. El Bejjani, R. & Hammarlund, M. Neural regeneration in Caenorhabditis elegans. *Annu.*

1065 *Rev. Genet.* **46**, 499–513 (2012).
1066 35. Kroehne, V., Freudenreich, D., Hans, S., Kaslin, J. & Brand, M. Regeneration of the adult
1067 zebrafish brain from neurogenic radial glia-type progenitors. *Development* **138**, 4831–
1068 4841 (2011).
1069 36. Hecker, A., Schulze, W., Oster, J., Richter, D. O. & Schuster, S. Removing a single
1070 neuron in a vertebrate brain forever abolishes an essential behavior. *Proc. Natl. Acad.*
1071 *Sci. U. S. A.* **117**, 3254–3260 (2020).
1072 37. Itayama, T. & Sawada, Y. Development of electrical activity in regenerating aggregates of
1073 hydra cells. *J. Exp. Zool.* **273**, 519–26 (1995).
1074 38. Soriano, J., Rüdiger, S., Pullarkat, P. & Ott, A. Mechanogenetic coupling of Hydra
1075 symmetry breaking and driven turing instability model. *Biophys. J.* **96**, 1649–1660 (2009).
1076 39. Gierer, A. *et al.* Regeneration of Hydra from Reaggregated Cells. *Nat. New Biol.* **239**, 98–
1077 101 (1972).
1078 40. Burnett, A. L. & Diehl, N. A. The nervous system of hydra. I. Types, distribution and origin
1079 of nerve elements. *J. Exp. Zool.* **157**, 217–226 (1964).
1080 41. Lfntz, T. L. & Barrnett, R. J. Fine structure of the nervous system. *Am. Zool.* (1965).
1081 42. Bode, H. R., Heimfeld, S., Koizumi, O., Llttlefield, C. L. & Yaross, M. S. Maintenance and
1082 regeneration of the nerve net in hydra. *Integr. Comp. Biol.* **28**, 1053–1063 (1988).
1083 43. Campbell, R. D. Tissue dynamics of steady state growth in hydra littoralis. III. Behavior of
1084 specific cell types during tissue movements. *J. Exp. Zool.* **164**, 379–391 (1967).
1085 44. Bode, H. *et al.* Quantitative analysis of cell types during growth and morphogenesis in
1086 Hydra. *Wilhelm Roux Arch. f□r Entwicklungsmechanik der Org.* **171**, 269–285 (1973).
1087 45. Epp, L. & Tardent, P. The distribution of nerve cells inHydra attenuata Pall. *Wilhelm*
1088 *Roux's Arch. Dev. Biol.* **185**, 185–193 (1978).
1089 46. Koizumi, O. *et al.* Nerve ring of the hypostome in Hydra. I. Its structure, development, and
1090 maintenance. *J. Comp. Neurol.* **326**, 7–21 (1992).

1091 47. Hufnagel, L. A. & Kass-Simon, G. The two nerve rings of the hypostomal nervous system
1092 of Hydra vulgaris---an immunohistochemical analysis. *Cell Tissue Res.* **366**, 1–15 (2016).
1093 48. Siebert, S. *et al.* Stem cell differentiation trajectories in Hydra resolved at single-cell
1094 resolution. *Science (80-.).* **365**, eaav9314 (2019).
1095 49. Mast, S. O. REACTIONS TO TEMPERATURE CHANGES IN SPIRILLUM, HYDRA, AND
1096 FRESH-WATER PLANARIANS. *Am. J. Physiol. Content* **10**, 165–190 (1903).
1097 50. Wagner, G. Memoirs: On Some Movements and Reactions of Hydra. *J. Cell Sci.* **s2-48**,
1098 585–622 (1905).
1099 51. Rushforth, N. B. Inhibition of contraction responses of hydra. *Integr. Comp. Biol.* **5**, 505–
1100 513 (1965).
1101 52. Rushforth, N. B. ., Burnett, A. L. . & Maynard, R. Behavior in Hydra : Contraction
1102 Responses of Hydra pirardi to Mechanical and Light Stimuli. *Am. Assoc. Adv. Sci.* **139**,
1103 760–761 (1963).
1104 53. Rushforth, N. B. & Burke, D. S. Behavioral and electrophysiological studies of Hydra. II.
1105 Pacemaker activity of isolated tentacles. **140**, 502–519 (1971).
1106 54. CAMPBELL, R. D., JOSEPHSON, R. K., SCHWAB, W. E. & RUSHFORTH, N. B.
1107 Excitability of nerve-free hydra. *Nature* **262**, 388–390 (1976).
1108 55. Takaku, Y. *et al.* Innexin gap junctions in nerve cells coordinate spontaneous contractile
1109 behavior in Hydra polyps. *Sci. Rep.* **4**, 1–8 (2014).
1110 56. Chalfie, M. *et al.* The neural circuit for touch sensitivity in Caenorhabditis elegans. *J.*
1111 *Neurosci.* **5**, 956–64 (1985).
1112 57. Wicks, S. R., Roehrig, C. J. & Rankin, C. H. A dynamic network simulation of the
1113 nematode tap withdrawal circuit: Predictions concerning synaptic function using
1114 behavioral criteria. *J. Neurosci.* **16**, 4017–4031 (1996).
1115 58. Vaidya, A. R., Pujara, M. S., Petrides, M., Murray, E. A. & Fellows, L. K. Lesion Studies in
1116 Contemporary Neuroscience. *Trends Cogn. Sci.* **23**, 653–671 (2019).

1117 59. Krug, K., Daniel Salzman, C. & Waddell, S. Understanding the brain by controlling neural
1118 activity. *Philos. Trans. R. Soc. B Biol. Sci.* **370**, 1–4 (2015).
1119 60. PASSANO, L. M. & McCULLOUGH, C. B. Co-ordinating systems and behaviour in hydra.
1120 I. Pacemaker system of the periodic contractions. *J. Exp. Biol. 41 643-664, 1964* 643–
1121 664 (1964).
1122 61. Pierobon, P. Regional modulation of the response to glutathione in Hydra vulgaris. *J.*
1123 *Exp. Biol.* **218**, 2226–32 (2015).
1124 62. Cazet, J. & Juliano, C. Oral Regeneration Is the Default Pathway Triggered by Injury in
1125 Hydra. *bioRxiv* 2020.07.06.189811 (2020). doi:10.1101/2020.07.06.189811
1126 63. Tursch, A., Bartsch, N. & Holstein, T. W. MAPK signaling links the injury response to
1127 Wnt-regulated patterning in Hydra regeneration. *bioRxiv*
1128 2020.07.06.189795 (2020). doi:10.1101/2020.07.06.189795
1129 64. Bode, H. R. Head regeneration in Hydra. *Dev. Dyn.* **226**, 225–236 (2003).
1130 65. Goel, T., Wang, R., Martin, S., Lanphear, E. & Collins, E.-M. S. Linalool acts as a fast and
1131 reversible anesthetic in Hydra. *PLoS One* **14**, e0224221 (2019).
1132 66. Yum, S. *et al.* A Novel Neuropeptide, Hym-176, Induces Contraction of the Ectodermal
1133 Muscle in Hydra. *Biochem. Biophys. Res. Commun.* **248**, 584–590 (1998).
1134 67. Noro, Y. *et al.* Regionalized nervous system in Hydra and the mechanism of its
1135 development. *Gene Expr. Patterns* (2019). doi:10.1016/J.GEP.2019.01.003
1136 68. Klimovich, A. *et al.* Prototypical pacemaker neurons interact with the resident microbiota.
1137 *Proc. Natl. Acad. Sci. U. S. A.* **117**, 17854–17863 (2020).
1138 69. Shimizu, H. & Fujisawa, T. Peduncle of Hydra and the heart of higher organisms share a
1139 common ancestral origin. *Genesis* **36**, 182–186 (2003).
1140 70. Szymanski, J. R. & Yuste, R. Mapping the Whole-Body Muscle Activity of Hydra vulgaris.
1141 *Curr. Biol.* **29**, 1807-1817.e3 (2019).
1142 71. Huang, L. *et al.* Relationship between simultaneously recorded spiking activity and

fluorescence signal in GCaMP6 transgenic mice. *Elife* **10**, e51675 (2021).

72. Rueden, C. T. *et al.* ImageJ2: ImageJ for the next generation of scientific image data. *BMC Bioinformatics* **18**, 529 (2017).

73. Schindelin, J. *et al.* Fiji: An open-source platform for biological-image analysis. *Nat. Methods* **9**, 676–682 (2012).

74. Tinevez, J. Y. *et al.* TrackMate: An open and extensible platform for single-particle tracking. *Methods* **115**, 80–90 (2017).

75. Livak, K. J. & Schmittgen, T. D. Analysis of relative gene expression data using real-time quantitative PCR and the 2-ΔΔCT method. *Methods* **25**, 402–408 (2001).

76. Core R Team. R: A Language and Environment for Statistical Computing. *R Foundation for Statistical Computing* **2**, https://www.R--project.org (2020).

Acknowledgements

We thank Dr. Rob Steele (UC Irvine), Dr. Christophe Dupre (Harvard University), and Dr. Rafael Yuste (Columbia University) for sharing transgenic *Hydra*. We also thank Dr. Guillaume Duret and Dr. Caleb Kemere for useful discussions. The promoter sequence for EF1a for generating transgenic *Hydra* was provided by Jack Cazet (UC Davis, Juliano lab), and the plasmid with GCAMP7b was cloned (and codon optimized) by GenScript. The open source USB valve controller was built based on the design by Rafael Gómez-Sjöberg, Microfluidics Lab, Lawrence Berkeley National Laboratory, Berkeley, CA 94720. This work is funded by NSF EDGE. K.N.B. is funded by a training fellowship from the Keck Center of the Gulf Coast Consortia on the NSF IGERT: Neuroengineering from Cells to Systems 1250104. We also thank the Rice Shared Equipment Authority and nanofabrication cleanroom facility where the devices were fabricated.

Competing interests

The authors declare no competing interests.

Figures

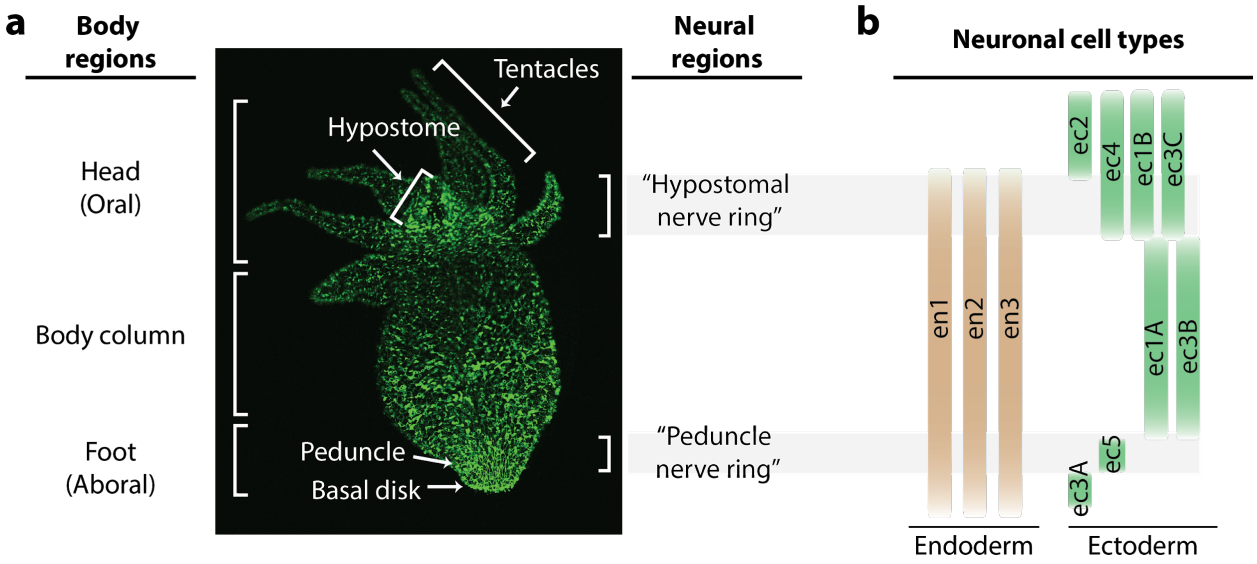

Figure 1: Distribution of neurons in the *Hydra* nerve net. a) Fluorescent image of *Hydra* nervous system. Green fluorescent protein (GFP) is expressed in neurons and neuronal progenitors (nGreen transgenic line[48]). Body anatomy is annotated on the left. White arrows indicate the body parts: hypostome, tentacles, peduncle, and basal disk. High neuronal density regions are annotated on the right. b) Distribution of neuronal cell types varying longitudinally along the body, with endodermal nerve net cell types in tan and ectodermal nerve net cell types in green. Cell types were identified through single cell RNA sequencing[48].

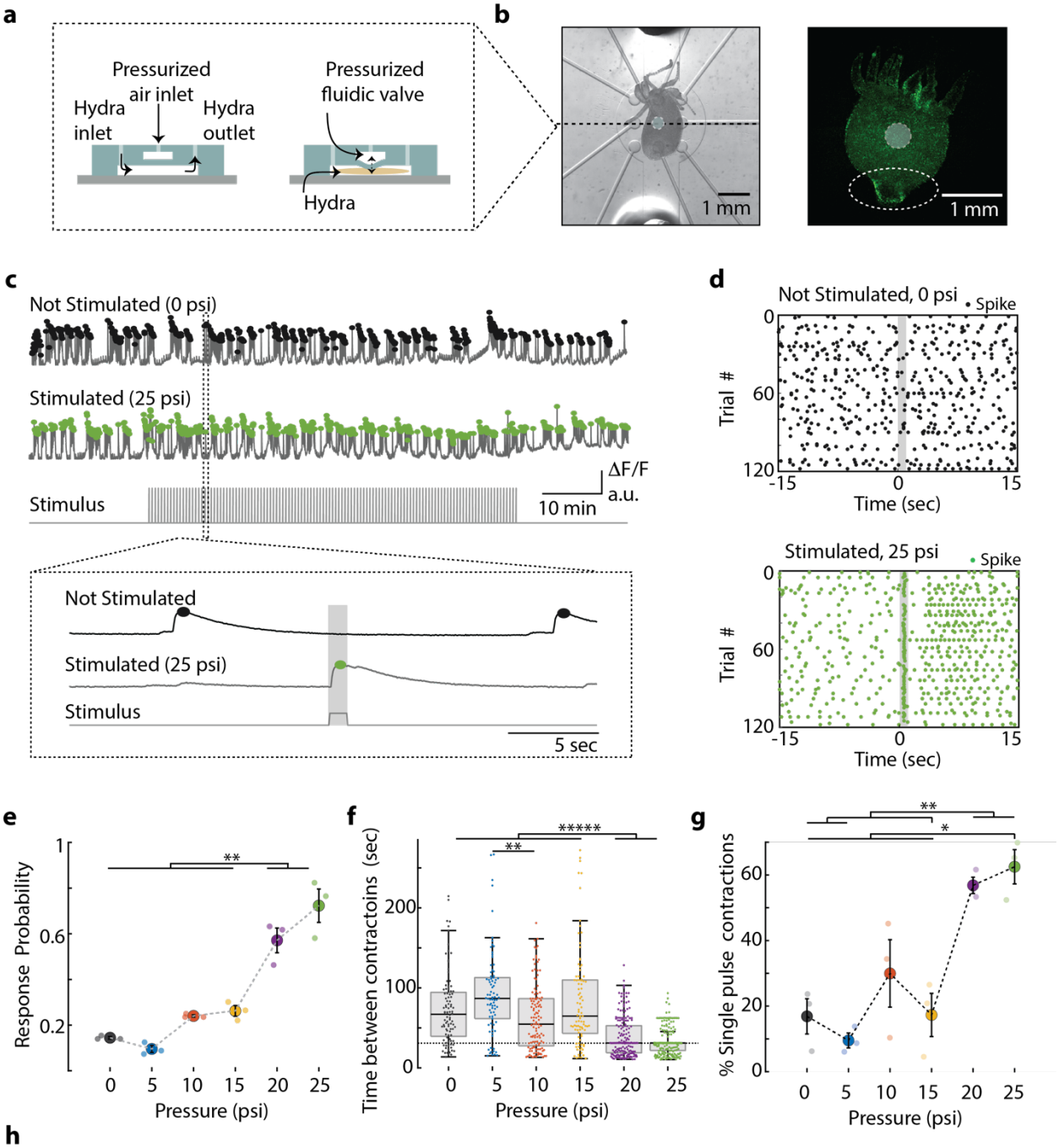

h

Pressure (psi)	Response probability mean +/- SEM	Time between contractions mean +/- SEM	Time between contractions median +/- SE	Single pulse contractions mean +/- SEM
0	0.11 +/- 0.01	72.98 +/- 4.58 sec	66.68 +/- 5.73 sec	16.87 +/- 5.38 %
5	0.09 +/- 0.02	92.66 +/- 5.87 sec	86.65 +/- 7.35 sec	9.52 +/- 2.27 %
10	0.23 +/- 0.01	63.01 +/- 3.73 sec	54.73 +/- 4.67 sec	29.96 +/- 10.29 %
15	0.24 +/- 0.03	83.60 +/- 6.37 sec	64.73 +/- 7.98 sec	17.30 +/- 6.59 %
20	0.60 +/- 0.06	38.28 +/- 1.77 sec	31.14 +/- 2.21 sec	56.84 +/- 2.48 %
25	0.77 +/- 0.08	32.20 +/- 1.04 sec	31.14 +/- 1.30 sec	62.50 +/- 5.23 %

1182 **Figure 2: *Hydra's* neuronal response depends on the mechanical stimulus intensity.** a) (left) Side view of double-layer
1183 microfluidic device for mechanical stimulation. (right) Device with pressurized valve. *Hydra* is immobilized in the bottom *Hydra* layer,
1184 and pressurized air supplied into the valve layer causes the circular membrane (400 µm diameter) to push down on *Hydra*. b) (left)
1185 Brightfield image of *Hydra* immobilized in the bottom layer of the chip and the arrangement of micro-valves on the top layer. Micro-
1186 valve used for stimulation falsely colored with a light blue circle. (right) Fluorescent image of *Hydra* with pan-neuronal expression of
1187 GCaMP6s. White dashed circle marks the peduncle region of interest (ROI) used for quantifying calcium fluorescence changes. c-d)
1188 Representative calcium fluorescence activity in the peduncle region from an animal not stimulated and animal mechanically
1189 stimulated with 25 psi. Black and green dots indicate fluorescence (calcium) spikes. Gray shaded regions indicate stimulus 'on' time
1190 (also "response window"). c) Fluorescence (calcium) trace from *Hydra* not stimulated (top) and stimulated with 25 psi (middle).
1191 Stimulation protocol in gray (bottom trace): 20 min no stimulation, 1 hr of repeated stimulation (1 sec 'on', 30 sec 'off') and 20 min no
1192 stimulation. Stimulus 'on' times indicated with vertical lines. Magnification of 30 sec fluorescence and stimulation protocol trace from
1193 one stimulation trial. d) Raster plot of stimulus time aligned spiking activity from multiple trials superimposed for *Hydra* not stimulated
1194 (top) and stimulated with 25 psi (bottom). e). Mechanosensory response probability, fraction of trials (out of 119 total) that have at
1195 least one calcium spike (also contraction pulse) occurring during the 1 sec response window (gray shaded region) when valve is
1196 pressurized. Large circles indicate average probability from all animals (N=3) combined for each condition. Small circles indicate
1197 probability from a single animal. Significant pairwise comparisons are shown with brackets (one-way ANOVA with post-hoc
1198 Bonferroni correction). f) Time interval between body contractions under each condition. Dashed line represents the time interval
1199 between stimuli (~31 sec). Brackets indicate significant differences in a Kruskal-Wallis test with post-hoc Dunn-Sidak correction. g)
1200 Percent of all body contractions that are a single pulse; brackets show significant pairwise comparisons from a one-way ANOVA
1201 with post-hoc Bonferroni correction. Error bars are standard error of mean (SEM); N = 3 *Hydra* for each condition; * = $p < 0.05$, ** =
1202 $p < 0.01$, ***** = $p < 0.00001$. h) Table summarizing the mechanosensory response probability, time between contractions, and
1203 percent of contractions that are single pulses for each stimulus intensity (mean ± SEM or median ± SE). Source data for the
1204 quantitative characterization of mechanosensory response are available in the Figure 2 – source data 1.
1205

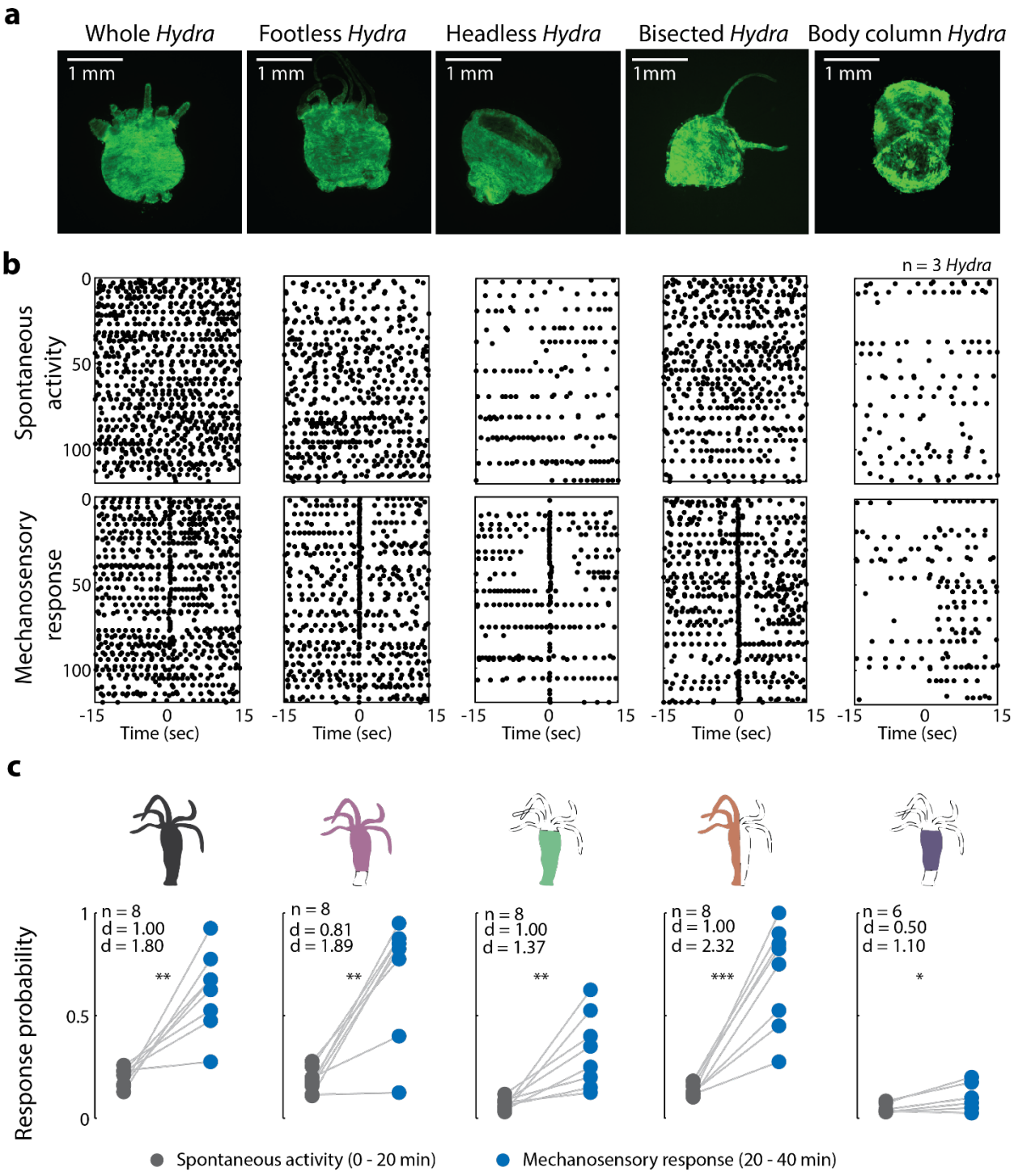
a
Whole Hydra
Footless Hydra
Headless Hydra
Bisected Hydra
Body column Hydra
1 mm
1 mm
1 mm
1mm
1 mm
b
n = 3 Hydra
Spontaneous activity
Mechanosensory response
0
50
100
-15
0
15
Time (sec)
c
Response probability
1
0.5
0
n = 8
d = 1.00
d = 1.80
**
n = 8
d = 0.81
d = 1.89
**
n = 8
d = 1.00
d = 1.37
**
n = 8
d = 1.00
d = 2.32
***
n = 6
d = 0.50
d = 1.10
*
Spontaneous activity (0 - 20 min)
Mechanosensory response (20 - 40 min)

1206

1207 **Figure 3: Oral region is important for mechanosensory response** a) Representative images of resection preparations (6-12
1208 hours post-resections) of transgenic *Hydra* during contraction (GCaMP7b, ectodermal epitheliomuscular cells): whole (or control),
1209 footless, headless, bisected and body column animal. Entire frame ROI was used for analysis of the whole-body epithelial calcium
1210 activity. b) Representative raster plot of stimulus time aligned calcium spikes from three animals with multiple trials superimposed.
1211 Each black dot is a peak in calcium fluorescence identified as a contraction pulse. c) Response probability, fraction of trials that
1212 have at least one calcium spike (also contraction pulse) occurring within 1 sec of stimulation onset. Gray dots are the mean
1213 contraction probability during no stimulation (t = 0-20 min) calculated from 1 sec window shifted by ~0.3 sec over 30 sec intervals.
1214 Blue dots are contraction probability during stimulation (t = 20-40 min) calculated from 1 sec response window during valve 'on'.
1215 Light gray lines connect the probabilities for spontaneous contraction and mechanosensory response for each individual. Cartoon
1216 schematics of *Hydra* indicate the resections performed. Excised body regions are outlined with a dashed line and unfilled area.
1217 Color filled body regions indicate the portion of *Hydra* retained for the experiment. P-values from a paired t-test indicated as follows:
1218 n.s. = not significant; * = $p < 0.05$; ** = $p < 0.01$; *** = $p < 0.001$. Source data for the mechanosensory response in resected animals
1219 are available in the Figure 3 – source data 1.
1220
1221

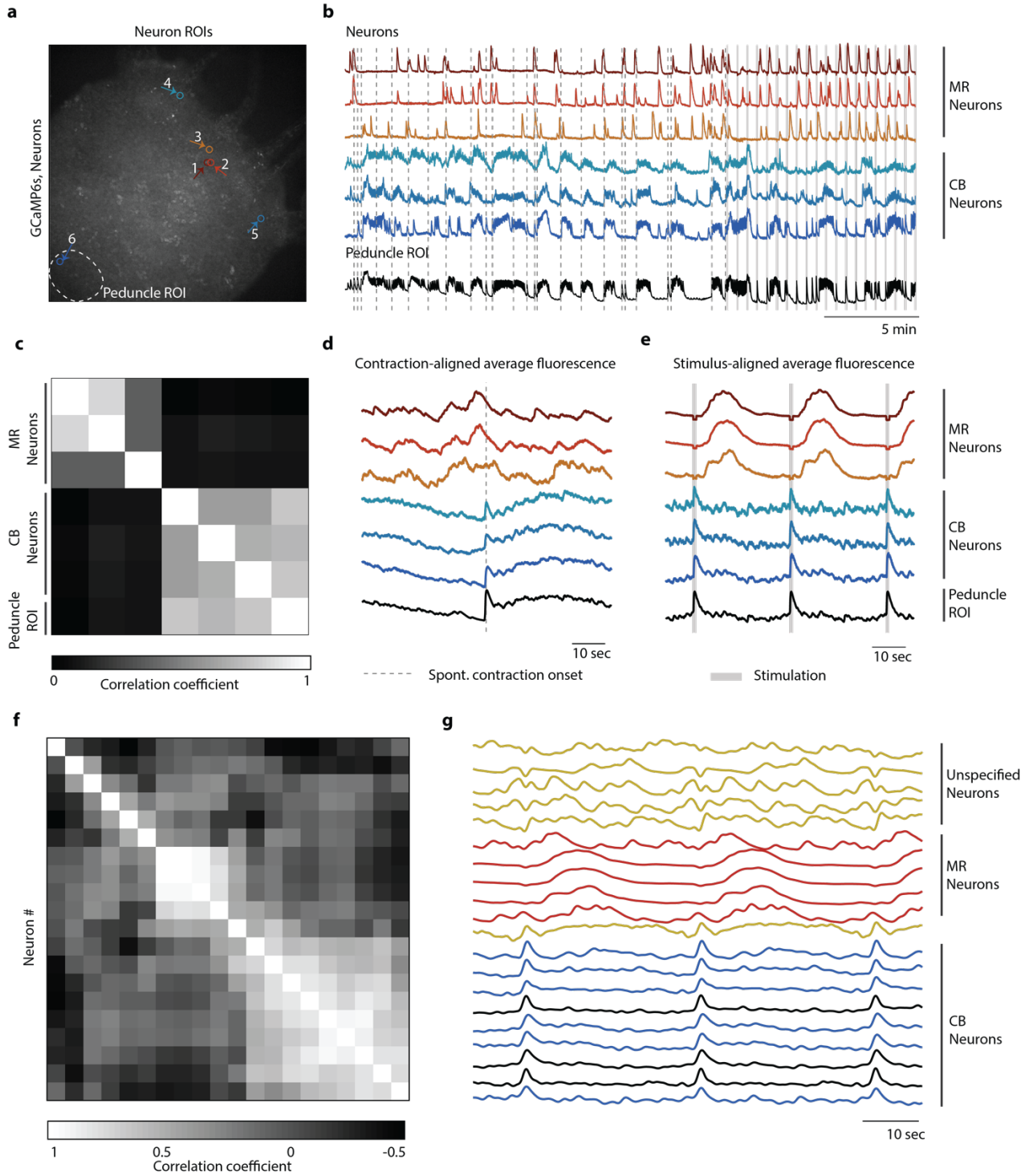

Figure 4: Distinct networks of neurons involved in spontaneous and stimulated behaviors. a) Fluorescent image of transgenic *Hydra* expressing GCaMP6s pan-neuronally. Individually tracked neurons ROIs are indicated by arrows, and peduncle ROI is outlined with a white dashed circle. b) Calcium fluorescence traces from single neurons (top 6 traces) and average calcium fluorescence from peduncle ROI (bottom trace). Mechanically responsive (MR) neurons are shown in shades of red. Contraction

burst (CB) neurons are shown in shades of blue. c) Heat map shows the correlation coefficients of individually tracked neurons and peduncle ROI from *Hydra* 1, with color bar at the bottom. Correlation was computed using the entire 30 min calcium fluorescence from single neurons shown in (b). d) Average calcium fluorescence traces from each of the neurons and peduncle ROI during spontaneous behaviors time-aligned with the onset of spontaneous body contractions. Dashed line indicates the onset of body contraction. e) Average calcium fluorescence traces from each of the neurons and peduncle ROI during stimulated behaviors time-aligned with the onset of mechanical stimulation. Gray shaded rectangle indicates mechanical stimulation. f) Heat map shows the correlation coefficients of g) the average calcium fluorescence traces from each of the neurons and peduncle ROI (traces in black) from three different *Hydra* during stimulated behaviors time-aligned with the onset of mechanical stimulation. Three groups of neurons were identified across the three *Hydra.* CB neurons (traces in blue), MR neurons (traces in red) and unspecified neurons (traces in yellow). a-e) Calcium fluorescence traces and correlation analysis (entire 30 min of activity, 20 min of spontaneous activity and 10 min of stimulated activity) from one representative *Hydra*. f-g) Correlation analysis of the average stimulus-aligned calcium fluorescence (30 sec stimulation interval average from 10 min of stimulated activity) of each neuron pooled multiple *Hydra* (N = 3 *Hydra*) to highlight the three groups of neurons identified: CB, MR and unspecified. Source data for fluorescent calcium activity from single neurons are available in the Figure 4 – source data 1.

1243 # Figure Supplements

1244

1245 **Figure 2 – Figure Supplement 1: Distribution of mechanical forces.** Fluorescent image (grayscale) of
1246 transgenic *Hydra* (nGreen) expressing GFP in neurons and neural progenitors. The Oral region is on the
1247 left. Aboral//peduncle region is on the right. Arrows (cyan) overlayed indicate the displacement of
1248 individual cells immediately before and after the valve is pressurized for stimulation (~50 msec). The
1249 lengths of the arrows are enlarged to be visible with the scaled size of the largest displacement ~31 μm
1250 as indicated by the legend (lower left). Semi-transparent (yellow) circle indicates the location of the valve
1251 (400 μm diameter). b) Displacement of neurons due to stimulation varies with the location of the neurons
1252 from the valve center. Each semi-transparent blue dot represents a single neuron (n= 222 neurons).
1253 Black dots (connected by black dashed line) represent the average displacement of the highest three
1254 displacements within a 50 μm radial band. Microfluidic valve has a radius of 200 μm indicated by the
1255 yellow shaded region. Majority of the cumulative displacement (>60 %) is localized to a 250 μm radius
1256 bordering the valve indicated by the blue dashed line at 450 μm. Neurons more than 750 μm from the
1257 microfluidic valve center have negligible displacement (<6% cumulative displacement) indicated by the
1258 green dashed line.

1259

1260

1261 **Figure 2 – Figure Supplement 2: Average calcium fluorescence from large peduncle ROI**
1262 **correlated with calcium fluorescence from smaller ROIs for individual peduncle neurons**. a)
1263 Fluorescent image of transgenic Hydra expressing GCaMP6s pan-neuronally. Dashed while circle
1264 indicates the peduncle ROI. Small cyan circles indicate the individual neuron ROIs. Peduncle region is in
1265 the top right. The oral end of the Hydra (not shown in the image) is oriented towards the bottom left
1266 corner. b) Average calcium fluorescence trace (black) from the large peduncle ROI. Average calcium
1267 traces (gray) from individual neurons in the peduncle.

1268

1269 **Figure 2 – Figure Supplement 3: Spikes in calcium fluorescence are due to calcium activity not**
1270 **motion artifacts.** a) Fluorescence image of transgenic *Hydra* (nGreen) expressing GFP in neurons false
1271 colored with hot green colormap. Neurons appear in white. b) Fluorescence image of transgenic *Hydra*

1272 expressing GCaMP6s in neurons false colored with hot green colormap. c) Fluorescence image of
1273 transgenic *Hydra* expressing GCaMP7b in ectodermal epitheliomuscular cells false colored with hot green
1274 colormap. a-c) Body length (white arrow), valve ROI (top circles), peduncle ROI (larger bottom circles)
1275 and whole frame ROI (entire frame square) annotated on all three images for comparison. d) Average
1276 body length trace time-aligned to stimulus onset from GFP *Hydra* (left) and GCaMP *Hydra* (middle, right).
1277 Light gray shaded region indicates when the stimulation is on. e) Average fluorescence trace calculated
1278 from the annotated peduncle ROI from GFP *Hydra* (left) and GCaMP *Hydra* (middle, right). f) Average
1279 fluorescence trace calculated from the whole frame ROI from GFP *Hydra* (left) and GCaMP *Hydra*
1280 (middle, right). g) Average fluorescence trace calculated from the annotated valve ROI from GFP *Hydra*
1281 (left) and GCaMP *Hydra* (middle, right).
1282
1283
1284 **Figure 2 – Figure Supplement 4: Simultaneous electrophysiology and calcium imaging of**
1285 **ectodermal epitheliomuscular cells.** (a) Photograph (left) of a microfluidic immobilization chamber filled
1286 with green dye. Black box highlights the recording region in the microfluidic chamber (110 μm tall). False
1287 colored scanning electron micrograph (middle) shows the recording region (blue, photoresist; light grey,
1288 Pt; dark grey, silica) on the nano-SPEAR chip (50 μm tall). Inset shows a zoom-in of the Pt electrode
1289 (light grey) suspended mid-way between the top and bottom of the photoresist sidewall (blue). Brightfield
1290 image (right) shows *Hydra* immobilized in the microfluidic chamber placed on top of the nano-SPEAR chip
1291 with combined 160 μm tall recording region (Reproduced from Figure 2A, Badhiwala et al, 2018[31] by
1292 permission of The Royal Society of Chemistry. This panel is not covered by the CC-BY 4.0 license, and
1293 further reproduction of this panel would need permission from the copyright holder.) b) Simultaneous
1294 electrophysiology and calcium imaging in transgenic *Hydra* (GCaMP6s, ectodermal epitheliomuscular
1295 cells). Top trace shows mean fluorescence ($\Delta F/F$) from ectodermal epitheliomuscular cells (whole frame
1296 ROI) in *Hydra* (GCaMP, ectodermal) (10Hz). Bottom trace shows simultaneously recorded electrical
1297 activity from the *Hydra* (1KHz). High and low activity periods identified based on peak amplitude. Inset:
1298 left box shows correlation during high activity period, contraction bursts. Traces show peaks in
1299 fluorescence (top trace) coinciding with peaks in electrophysiology (bottom trace). A representative

1300 fluorescence image shows high levels of fluorescence thus calcium activity in the entire body during
1301 contraction burst events. Correlation map spatially plotting the correlation coefficient shows the entire
1302 body has calcium activity correlated with electrophysiology. Inset: right box shows correlation during low
1303 activity period, tentacle pulses. Traces show peaks in fluorescence (top trace) coinciding with peaks in
1304 electrophysiology (bottom trace). A representative fluorescence image shows high levels of fluorescence
1305 in the tentacle region during tentacle pulses. Cross correlation map shows the tentacle region has
1306 calcium activity correlated with electrophysiology. Almost all spikes in electrophysiology coincide with
1307 spike in fluorescence from ectodermal epitheliomuscular cells (and behavioral contractions).
1308
1309
1310 **Figure 2 – Figure Supplement 5: *Hydra*'s epitheliomuscular response is dependent on the**
1311 **mechanical stimulus intensity**. a) Gray trace (top) is the stimulation protocol. 20 min no stimulation, 20
1312 min of repeated stimulation (1 sec 'on', 30 sec 'off') at 15 psi, 20 min of repeated stimulation (1 sec 'on',
1313 30 sec 'off') at 20 psi, and 20 min of repeated stimulation (1 sec 'on', 30 sec 'off') at 25 psi. Stimulus 'on'
1314 times indicated by vertical lines. Entire frame ROI used for analysis of the whole-body epithelial calcium
1315 activity. Representative calcium fluorescence trace (blue) from ectodermal epitheliomuscles (GCaMP7b)
1316 from animal stimulated with three different stimulus intensities for 20 min each (15, 20 and 25 psi).
1317 Representative calcium fluorescence trace (teal) from ectodermal epitheliomuscles (GCaMP7b) from
1318 animal stimulated with three different stimulus intensities for 20 min each (25, 20 and 15 psi). The
1319 decrease in fluorescence amplitude observed for both increasing in and decreasing stimulus intensity is
1320 due to photobleaching of the calcium indicator. b) Mechanosensory response probability at different
1321 stimulus intensities (N = 3 animals). Response probability, fraction of trials that have at least one calcium
1322 spike (also contraction pulse) occurring within 1 sec of stimulation onset.
1323
1324
1325 **Figure 2 – Figure Supplement 6: Mechanosensory response window.** a) Different response windows
1326 tested (1 sec in blue; 5 sec in orange; 10 sec in yellow; and 15 sec in purple) (Top). The lengths of the
1327 rectangles correspond to time (sec) in the raster plot below. Stimulus trace in gray. Representative raster

1328 plot of time-aligned contraction pulses from multiple trials superimposed from one animal stimulated at 20
1329 psi every 31 sec for 60 min (Bottom). Each black dot is a spike in calcium fluorescence identified as a
1330 contraction pulse. Stimulus is applied from 0 - 1 sec as indicated by a step in stimulus trace. b) Response
1331 probability, fraction of trials that have at least one calcium spike (also contraction pulse) occurring during
1332 different response windows (1 sec in blue; 5 sec in orange; 10 sec in yellow; and 15 sec in purple within
1333 stimulation onset).
1334
1335
1336 **Figure 2 – Figure Supplement 7: Mechanical sensitivity of different body regions in *Hydra*.** a)
1337 Response probability of transgenic Hydra (N=3 animals expressing GCaMP6s in neurons) stimulated at
1338 three different body regions: Oral, Mid-body and Aboral. Annotated Hydra below the plot indicates the
1339 three stimulation regions used. b) Response probability of transgenic Hydra (n=8 animal expressing
1340 GCaMP7b in ectodermal epitheliomuscular cells) Response probability is calculated using average
1341 calcium fluorescence from neurons in the peduncle ROI in a) and using average calcium fluorescence
1342 from the ectodermal epitheliomuscular cells from the entire body in b) and c).
1343
1344
1345 **Figure 2 – Figure Supplement 8: *Hydra's* mechanosensory response time is faster than passive**
1346 **calcium diffusion through epitheliomuscular cells** a) Distance calcium diffuses passively over given
1347 time (left, black line plot) approximated using passive diffusion equation (right). Light brown shaded
1348 region indicates the range of body length (~ 0.5 - 1 mm) of *Hydra* in microfluidic chambers used for the
1349 experiments. Teal shaded region indicates the average time between stimulus onset and observed spike
1350 in fluorescence (mean response time 0.5 - 1 sec). Yellow shaded region is the theoretical mean calcium
1351 diffusion time calculated assuming passive diffusion. b-e) Mean calcium fluorescence time-aligned to
1352 stimulus and normalized. Stimulus is applied at 0 sec (valve 'on' from 0 - 1 sec). b) Mean calcium activity
1353 from the peduncle network of neurons at different stimulus intensities. c) Mean calcium activity from
1354 ectodermal epitheliomuscular cells at different stimulus intensities. b-c) The line colors correspond to
1355 different stimulus intensities shown at the bottom. d) Mean calcium activity from peduncle network of

1356 neurons in different body resections stimulated at 20 psi (pressure for ~ 60% response probability in
1357 whole animals). e) Mean calcium activity from ectodermal epitheliomuscular cells in different body
1358 resections different body resections stimulated at 22 psi (pressure for ~ 60% response probability in
1359 whole animals). d-e) The line colors correspond to the different resections shown at the bottom with
1360 cartoon schematic of the resected *Hydra* with the same color.
1361
1362
1363 **Figure 2 – Figure Supplement 9: Long-term mechanical stimulation** a) Representative calcium
1364 fluorescence trace from the peduncle region from an animal (GcaMP6s, neurons) not stimulated and
1365 animal mechanically stimulated with 20 psi. Stimulus protocol in gray, 20 min no stimulation, 120 min of
1366 repeated stimulation (1 sec 'on', 30 sec 'off') at 20 psi followed by no stimulation. b) Spontaneous and
1367 stimulated (mechanosensory response) contraction pulse probabilities for the first and second hour of
1368 stimulation compared for each animal. Gray circles are mean contraction pulse probability during no
1369 stimulation calculated from an average of 1 sec window shifted by ~ 0.3 sec over 30 sec intervals (N = 3).
1370 Blue circles are contraction probability during stimulation calculated from 1 sec response window during
1371 valve 'on' (N = 2). Light gray lines indicate the change in probabilities from hour 1 to hour 2 for each
1372 individual. (paired t-test, n.s. = not significant)
1373
1374
1375 **Figure 3 – Figure Supplement 1: Regeneration of the peduncle network.** a) Summary schematic of
1376 the experiment performed. Dashed line indicates where the incision was made to remove the lower half of
1377 the transgenic *Hydra* body (GcaMP6s, neurons) to discover when the peduncle neuronal network is
1378 regenerated. b) Fluorescence images of "footless" *Hydra* during body contractions at various timepoints t
1379 = 1 hr, 5 hr and 9 hr after bisection. Pink arrow indicates the open wound visible at t = 1 hr but not at
1380 other timepoints. c) Fluorescence images of another "footless" *Hydra* during body contractions at various
1381 timepoints t = 37 hr, 39 hr, 41 hr. Blue dashed circle indicates the region where the peduncle network is
1382 found. Blue arrows indicate some of the neurons in the peduncle network with clearly well-connected
1383 neurons at t = 41 hr.

1384

1385

1386 **Figure 3 - Figure Supplement 2: RT-qPCR analyses of neuron subtype-specific gene expression in**
1387 **resected animals demonstrates loss of specific neuron subtypes.** RT-qPCR was used to test for the
1388 loss of specific neuron subtypes in whole, tube (no head or foot), headless, footless, and bisected *Hydra*
1389 using uniquely expressed biomarkers for each subtype. There is not a specific biomarker for ec3A
1390 (located in the basal disk), so the marker used to test for the presence or absence of this cell type is also
1391 expressed in ec3B (located in the body column). Therefore, expression of the ec3A/B marker gene is
1392 reduced, but not completely lost in animals with resected feet ("tube" and "footless"). However, ec5
1393 expression (located in the peduncle above the basal disk) is completely lost in animals with resected feet,
1394 thus it is clear that the ec3A subtype is completely lost in these animals. Biomarkers for neuron subtypes
1395 located in the head and tentacles (ec1B, ec2, ec3C, ec4) are completely lost in animals with resected
1396 heads ("headless" and "tube"). Data were analyzed with the $2^{\wedge -\Delta\Delta Ct}$ method and results were normalized to
1397 the housekeeping gene *RP49* and to expression in whole animals.

1398

1399

1400 **Figure 3 – Figure Supplement 3: Mechanosensory response from ectodermal epitheliomuscular**
1401 **cells and neurons in resected *Hydra*.** a) Representative images of resection preparations of transgenic
1402 *Hydra* (GCaMP7b, ectodermal epitheliomuscular cells: whole (or control), "footless", "headless",
1403 "bisected", and "body column". White dashed square indicates the whole frame ROI used for quantifying
1404 response. b) Spontaneous probability of at least one spiking event (or contraction pulse) occurring during
1405 a random 1 sec window. (1 sec window slide by ~ 0.3 sec across 30 sec stimulation intervals; Kruskal-
1406 Wallis test with post hoc dunn-sidak correction) c) Mechanosensory response probability during 1 sec of
1407 valve on (Response probability, fraction of trials that have at least one calcium spike (also contraction
1408 pulse) occurring within 1 sec of stimulation onset). Large circles indicate average values from all animals
1409 combined for each condition. Small circles indicate probability from individual animals (one-way anova
1410 with post hoc Bonferroni correction). Error bars are standard error of mean (S.E.M.) (N = 3 *Hydra* for each
1411 condition; analysis from 60 min of stimulation which is imaging t = 20 – 80 min; n.s. = not significant, ** =

1412 p < 0.01, **** = p < 0.0001, ***** = p < 0.00001). d) Representative images of resection preparations of
1413 transgenic *Hydra* (GCaMP6s, neurons: whole (or control), “headless”, and “bisected”. White dashed circle
1414 indicates the peduncle ROI used for quantifying response. e) Spontaneous probability of at least one
1415 spiking event (or contraction pulse) occurring during a random 1 sec window. (1 sec window slide by ~
1416 0.3 sec across 30 sec stimulation intervals; Kruskal-Wallis test with post hoc dunn-sidak correction) f)
1417 Mechanosensory response probability during 1 sec of valve on. Large circles indicate average values
1418 from all animals combined for each condition. (Response probability, fraction of trials that have at least
1419 one calcium spike (also contraction pulse) occurring within 1 sec of stimulation onset.) Small circles
1420 indicate probability from individual animals (one-way anova with post hoc Bonferroni correction). Error
1421 bars are standard error of mean (S.E.M.) (N = 3 *Hydra* for each condition; analysis from 60 min of
1422 stimulation which is imaging t = 20 – 80 min; n.s. = not significant, ** = p < 0.01, **** = p < 0.0001, ***** =
1423 p < 0.00001).
1424
1425
1426 **Figure 3 – Figure Supplement 4: Contraction activity in non-stimulated animals.** Cartoon schematic
1427 of resection preparations of transgenic *Hydra* (GCaMP7b, ectodermal epitheliomuscular cells): whole (or
1428 control), “footless”, “headless”, “bisected” and “body column” animals. Entire frame ROI used for analysis
1429 of the whole-body epithelial calcium activity. Gray circles are mean contraction probability during t = 0 - 20
1430 min. Blue circles are mean contraction probability during t = 20 - 40 min, (this time corresponds to when
1431 stimulated animals receive mechanical stimuli). Mean probability calculated from 1 sec window shifted by
1432 ~ 0.3 sec over 30 sec intervals. (Response probability, fraction of trials that have at least one calcium
1433 spike (also contraction pulse) occurring within 1 sec of stimulation onset). Pressure in valves = 0 psi. Light
1434 gray lines pair the spontaneous contractions probability from the first 20 min interval with the second 20
1435 min interval from each individual animal. (Whole N = 4, footless N = 3, headless N = 3, bisected N = 5,
1436 body column N = 3 *Hydra*, paired t-test, n.s. = not significant)
1437
1438

1439 **Figure 3 – Figure Supplement 5: Hypostome and peduncle nerve rings work together to**
1440 **coordinate contractile behavior** a) Representative fluorescence trace used to calculate time interval
1441 between contractions. b) Time interval between spontaneous contractions in animals with different
1442 resections: whole, “footless”, “headless”, “bisected” and “body column”. c) Time interval between
1443 stimulated contractions in animals with different resections. d) Representative fluorescence trace used to
1444 calculate time interval between contraction pulses. For illustration purpose, only a select few of the time
1445 intervals are shown. e) Time interval between spontaneous contraction pulses in animals with different
1446 resections. f) Time interval between stimulated contraction pulses in animals with different resections. g)
1447 Representative fluorescence trace used to calculate contraction duration. h) Duration of spontaneous
1448 contractions in animals with different resections. i) Duration of stimulated contractions in animals with
1449 different resections. N= 3 *Hydra* (GcaMP7b, Ectodermal epitheliomuscles) per resection. (Kruskal-Wallis
1450 test with dunn-sidak correction, n.s. = not significant, ** = $p < 0.01$, *** = $p < 0.001$, **** = $p < 0.0001$,*****
1451 = $p < 0.00001$,****** = $p < 0.000001$)
1452
1453
1454 **Figure 4 – Figure Supplement 1: Single cell correlation analysis.** a) Fluorescence image of
1455 transgenic *Hydra* (#2) expressing GCaMP6s pan-neuronally. Individually tracked neuronal ROIs are
1456 indicated with circles. The neurons are numbered in the order their traces are appear in c-e with the same
1457 colors. Peduncle ROI outlined with white dashed line. b) Calcium fluorescence traces from single neurons
1458 (top 6 traces) and average calcium fluorescence from peduncle ROI (bottom trace). Mechanically
1459 responsive (MR) neurons are shown in shades of red. Contraction burst (CB) neurons are shown in
1460 shades of blue. Unspecified neurons are shown in yellow, and their activity do not resemble any of the
1461 previously identified neuronal networks (contraction burst, rhythmic potential or the mechanically
1462 responsive reported here). c) Heat map shows the correlation coefficients of individually tracked neurons
1463 and peduncle ROI. Colorbar is at the bottom. d) Average calcium fluorescence traces from each of the
1464 neurons and peduncle ROI during spontaneous behaviors time-aligned with the onset of spontaneous
1465 body contractions. Dashed line indicates the onset of body contraction. e) Average calcium fluorescence

1466 traces from each of the neurons and peduncle ROI during stimulated behaviors time-aligned with the
1467 onset of mechanical stimulation. Gray shaded rectangle indicates mechanical stimulation.
1468
1469
1470 **Figure 4 – Figure Supplement 2: Single cell correlation analysis.** a) Fluorescence image of
1471 transgenic *Hydra* (#3) expressing GCaMP6s pan-neuronally. Individually tracked neuronal ROIs are
1472 indicated with circles. The neurons are numbered in the order their traces are appear in c-e with the same
1473 colors. Peduncle ROI outlined with white dashed line. b) Calcium fluorescence traces from single neurons
1474 (top 5 traces) and average calcium fluorescence from peduncle ROI (bottom trace). Mechanically
1475 responsive (MR) neurons are shown in shades of red. Contraction burst (CB) neurons are shown in
1476 shades of blue. Unspecified neurons are shown in yellow, and their activity do not resemble any of the
1477 previously identified neuronal networks (contraction burst, rhythmic potential or the mechanically
1478 responsive reported here). c) Heat map shows the correlation coefficients of individually tracked neurons
1479 and peduncle ROI. Colorbar is at the bottom. d) Average calcium fluorescence traces from each of the
1480 neurons and peduncle ROI during spontaneous behaviors time-aligned with the onset of spontaneous
1481 body contractions. Dashed line indicates the onset of body contraction. e) Average calcium fluorescence
1482 traces from each of the neurons and peduncle ROI during stimulated behaviors time-aligned with the
1483 onset of mechanical stimulation. Gray shaded rectangle indicates mechanical stimulation.
1484
1485
1486 **Figure 4 – Figure Supplement 3: Random shuffling of single cell correlation analysis.** Individual
1487 neuronal fluorescence time-series were randomly shuffled to show the correlation coefficients were not
1488 due to random chance in all three *Hydra* (each row is a different *Hydra*). Original correlation coefficients
1489 from 10 mins of raw fluorescence time-series (a-c), shuffled correlation coefficients from randomly
1490 reshuffled blocks reconstructing 10 mins of fluorescence time-series (d-e) and z-score of correlation
1491 coefficients calculated based on random reshuffling (g-i). Original correlation coefficients were calculated
1492 from the 10 mins of raw fluorescence activity for each of the neurons during mechanical stimulation.
1493 Shuffled correlation coefficients were calculated by taking the mean of correlation coefficients from

randomly reshuffled fluorescence time-series. Briefly, the raw fluorescence time-series from 10 mins of mechanical stimulation was divided into 100 blocks, which were then randomly recombined for each of the neurons to calculated correlation coefficients and this random reshuffling was repeated 1000 times. Z-score was calculated using the mean and standard deviation of the correlation coefficients calculated from random reshuffling repeated 1000 times. The heatmap for z-score (g-i) resemble the original correlation coefficients (a-c) indicating the correlation coefficients of the raw fluorescence time-series were not a result of random chance. Except for the diagonals which represents autocorrelation, the mean correlation coefficients resulting from randomly reshuffled fluorescence (e-f) are zero for all neuron pairs indicating the correlation due to random chance.

1504 **Description of Videos**

1505 **Video 1:**

1506 Microfluidic system to study mechanosensory response in *Hydra*. Dashed blue circle indicates the
1507 microfluidic valve that presses down on *Hydra.* Mechanosensory response from neurons and
1508 epitheliomuscular cells is shown.

1509

1510 **Video 2:**

1511 Spontaneous neural calcium activity in normal animals. Dashed blue circle indicates the ROI used for
1512 calcium trace shown in blue (bottom). (Playback 100x.)

1513

1514 **Video 3:**

1515 Stimulated neural calcium activity in normal animals. Dashed blue square indicates the ROI used for
1516 calcium trace shown in blue (bottom). Dashed white circle indicates the location of the valve that presses
1517 down on *Hydra* when inflated. Gray trace shows the stimulus protocol, where vertical lines indicate valve
1518 'on' times. Stimulus applied beginning t = ~ 20 min and ends t = ~80 min. Valve is 'on' for 1 sec and 'off'
1519 for 30 sec. (Playback 100x.)

1520

1521 **Video 4:**

1522 Spontaneous ectodermal epitheliomuscular calcium activity in normal animals. Dashed blue square
1523 indicates the ROI (entire frame) used for the calcium trace shown in blue (bottom). (Playback 100x.)

1524

1525 **Video 5:**

1526 Stimulated ectodermal epitheliomuscular calcium activity in normal animals. Dashed blue square
1527 indicates the ROI (entire frame) used for calcium trace shown in blue (bottom). Dashed white circle
1528 indicates the location of the valve that presses down on *Hydra* when inflated. Gray trace shows the
1529 stimulus protocol, where vertical lines indicate valve 'on' times. Stimulus applied beginning t = ~ 20 min
1530 and ends t = ~80 min. Valve is 'on' for 1 sec and 'off' for 30 sec. (Playback 100x.)

1531

Video 6:

Spontaneous neural calcium activity in longitudinally bisected animals. Dashed blue circle indicates the ROI used for calcium trace shown in blue (bottom). (Playback 100x.)

Video 7:

Stimulated neural calcium activity in longitudinally bisected animals. Dashed blue circle indicates the ROI used for calcium trace shown in blue (bottom). Dashed white circle indicates the location of the valve that presses down on *Hydra* when inflated. Gray trace shows the stimulus protocol, where vertical lines indicate valve 'on' times. Stimulus applied beginning t = ~ 20 min and ends t = ~80 min. Valve is 'on' for 1 sec and 'off' for 30 sec. (Playback 100x.)

Video 8:

Spontaneous neural calcium activity in headless animals. Dashed blue circle indicates the ROI used for calcium trace shown in blue (bottom). Animal is less active without the head and fewer spikes in calcium activity of peduncle neurons are observed. (Playback 100x.)

Video 9:

Stimulated neural calcium activity in headless animals. Dashed blue circle indicates the ROI used for calcium trace shown in blue (bottom). Dashed white circle indicates the location of the valve that presses down on *Hydra* when inflated. Gray trace shows the stimulus protocol, where vertical lines indicate valve 'on' times. Stimulus applied beginning t = ~ 20 min and ends t = ~80 min. Valve is 'on' for 1 sec and 'off' for 30 sec. Animal is less active without the head and fewer spikes in calcium activity of peduncle neurons are observed without stimulation. After stimulation begins, more single pulse contractions occur. (Playback 100x.)

Video 10:

1559 Spontaneous ectodermal epitheliomuscular calcium activity in footless animals. Dashed blue square
1560 indicates the ROI (entire frame) used for the calcium trace shown in blue (bottom). (Playback 100x.)
1561
1562 **Video 11:**
1563 Stimulated ectodermal epitheliomuscular calcium activity in footless animals. Dashed blue square
1564 indicates the ROI (entire frame) used for calcium trace shown in blue (bottom). Dashed white circle
1565 indicates the location of the valve that presses down on *Hydra* when inflated. Gray trace shows the
1566 stimulus protocol, where vertical lines indicate valve 'on' times. Stimulus applied beginning t = ~ 20 min
1567 and ends t = ~80 min. Valve is 'on' for 1 sec and 'off' for 30 sec. (Playback 100x.)
1568
1569 **Video 12:**
1570 Spontaneous ectodermal epitheliomuscular calcium activity in headless animals. Dashed blue square
1571 indicates the ROI (entire frame) used for the calcium trace shown in blue (bottom). Animal is less active
1572 without the head and fewer spikes in calcium activity of the whole body ectodermal epitheliomuscular
1573 cells are observed. (Playback 100x.)
1574
1575 **Video 13:**
1576 Stimulated ectodermal epitheliomuscular calcium activity in headless animals. Dashed blue square
1577 indicates the ROI (entire frame) used for calcium trace shown in blue (bottom). Dashed white circle
1578 indicates the location of the valve that presses down on *Hydra* when inflated. Gray trace shows the
1579 stimulus protocol, where vertical lines indicate valve 'on' times. Stimulus applied beginning t = ~ 20 min
1580 and ends t = ~80 min. Valve is 'on' for 1 sec and 'off' for 30 sec. Animal is less active without the head
1581 and fewer spikes in calcium activity of epitheliomuscular cells are observed without stimulation. After
1582 stimulation begins, more single pulse contractions occur. (Playback 100x.)
1583
1584 **Video 14:**
1585 Spontaneous ectodermal epitheliomuscular calcium activity in bisected animals. Dashed blue square
1586 indicates the ROI (entire frame) used for the calcium trace shown in blue (bottom). Animal is less active

without the head and fewer spikes in calcium activity of the whole body ectodermal epitheliomuscular cells are observed. (Playback 100x.)

Video 15:

Stimulated ectodermal epitheliomuscular calcium activity in bisected animals. Dashed blue square indicates the ROI (entire frame) used for calcium trace shown in blue (bottom). Dashed white circle indicates the location of the valve that presses down on *Hydra* when inflated. Gray trace shows the stimulus protocol, where vertical lines indicate valve 'on' times. Stimulus applied beginning t = ~ 20 min and ends t = ~80 min. Valve is 'on' for 1 sec and 'off' for 30 sec. Animal is less active without the head and fewer spikes in calcium activity of epitheliomuscular cells are observed without stimulation. After stimulation begins, more single pulse contractions occur. (Playback 100x.)

Video 16:

Spontaneous ectodermal epitheliomuscular calcium activity in body column animals. Dashed blue square indicates the ROI (entire frame) used for the calcium trace shown in blue (bottom). Animal is less active without the head and fewer spikes in calcium activity of the whole body ectodermal epitheliomuscular cells are observed. (Playback 100x.)

Video 17:

Stimulated ectodermal epitheliomuscular calcium activity in body column animals. Dashed blue square indicates the ROI (entire frame) used for calcium trace shown in blue (bottom). Dashed white circle indicates the location of the valve that presses down on *Hydra* when inflated. Gray trace shows the stimulus protocol, where vertical lines indicate valve 'on' times. Stimulus applied beginning t = ~ 20 min and ends t = ~80 min. Valve is 'on' for 1 sec and 'off' for 30 sec. Animal is less active without the head and fewer spikes in calcium activity of epitheliomuscular cells are observed without stimulation. After stimulation begins, more single pulse contractions occur. (Playback 100x.)

Video 18:

1615 Stimulated neural calcium activity in the hypostome and body column of normal animals. Dashed blue
1616 circle indicates the ROI used for calcium trace shown in blue (bottom). Dashed white circle indicates the
1617 location of the valve that presses down on *Hydra* when inflated. Gray trace shows the stimulus protocol,
1618 where vertical lines indicate valve 'on' times. Stimulus applied beginning t = ~ 20 min, Valve is 'on' for 1
1619 sec and 'off' for 30 sec. Imaged with 10x 0.45 N.A. objective (Playback 100x.)
1620

Source data

Figure 2 – source data 1: source file for stimulus dependent mechanosensory response.

The file (Fig2_SourceData.mat) contains all source data used for quantitatively characterizing mechanosensory response shown in Figure 2. The file contains a struct named 'HydraData' with each trial in a different row. The columns contain the raw and processed data for each trial: 'StimCondition' indicates the stimulation pressure (0, 5, 10, 15, 20 or 25 psi) used during the trial; 'RawFluorescenceFoot' contains the raw fluorescence values from foot/peduncle ROI; 'StimulationTrace' contains the trace of stimulus delivery where 0 is valve off, 1 is valve on (and stimulation is being applied) per frame; 'Response Probability' is extracted after processing 'RawFluorescenceFoot' with stimulation onset times from 'StimulationTrace'; 'TimeBetweenContractions' is time in seconds between contraction burst pulses extracted from 'RawFluorescenceFoot'; 'SinglePulseContractions_Percent' is the percent of body contractions that occur as single pulses extracted from 'RawFluorescenceFoot'

Figure 3 – source data 1: source file mechanosensory response in resected animals.

The file (Fig3_SourceData.mat) contains all source data used for characterizing mechanosensory response in resected animals in Figure 3. The file contains a struct named 'HydraData' with each trial in a different row. The columns contain the raw and processed data for each trial: 'StimCondition' indicates stimulation condition (w/ or w/o stimulation; body resections - whole, bisected, no foot = Footless, no head = Headless, no head and foot = BodyColumn); 'RawFluorescenceFoot' contains the raw fluorescence values from foot/peduncle ROI; 'StimulationTrace' contains the trace of stimulus delivery where 0 is valve off, 1 is valve on (and stimulation is being applied) per frame; 'Response Probability' is the stimulated contraction probability extracted after processing 'RawFluorescenceFoot' with stimulation onset times from 'StimulationTrace'; 'BasalContractionProbability' is spontaneous contraction probability extracted after processing 'RawFluorescenceFoot' during (t = 0-20 min) the initial acclimation period without stimulation.

Figure 4 – source data 1: source file for fluorescent calcium activity from single neuron ROIs.

The file (Fig4_SourceData.zip) contains three folders ‘Hydra1’, ‘Hydra2’ and ‘Hydra3’ for the three different animals with individually tracked single neurons. Each folder contains a file called ‘IndividualNeuronTraces.mat’ with three different matrices: ‘NeuronROI_RawFluorAllFrames’ matrix [# of rows = # of neurons+1, # of columns = # of frames] contain the raw fluorescence intensities individual neuronal ROIs. Each row is different neuron and the last row in the matrix is the average fluorescence from peduncle ROI’; ‘ROI_xLocAllFrames’ matrix [# of rows = # of neurons, # of columns = # of frames] contains the x position of the center of circular ROIs for individual neurons; ‘ROI_yLocAllFrames’ matrix [# of rows = # of neurons, # of columns = # of frames] contains the y position of the center of circular ROIs for individual neurons